WIRELESS POWER TRANSFER FOR RAILWAY APPLICATIONS

by

Xiwen Xu

A dissertation submitted to the faculty of
the University of North Carolina at Charlotte
in partial fulfillment of the requirements
for the degree of Doctor of Philosophy in
Electrical Engineering

Charlotte

2022

Approved by:

____
Dr. Tiefu Zhao

____
Dr. Robert Cox

____
Dr. Michael Mazzola

____
Dr. Shen-En Chen

ABSTRACT

XIWEN XU. Wireless power transfer for railway applications. (Under the direction of DR. TIEFU ZHAO)

The United States trains have the highest energy demands in rail transport in the world. More than 90% of the trains are powered by diesel, which aggressively impacts climate change. Thus, railway system electrification is a trend to reduce the speed of global warming and realize carbon zero emissions. In addition, the current procedure of charging an electric locomotive is more complicated compared with charging an electric vehicle (EV). Thus, Inductive power transfer (IPT) technology has a huge potential for charging locomotives wirelessly.

IPT technology has been extensively studied for EV application in the past decades. However, it has not drawn much attention to railway applications. Due to the unique requirements of the railway system, most of the EV coupler designs are not directly compatible with wireless charging applications for a train. To fill this technical gap, this dissertation discusses the design considerations for railway application and introduces a design of a modular 5-kW IPT system for rail locomotives. According to the design constraints, a novel W-I coupler is proposed for the 5-kW IPT system, and the system is optimized via ANSYS Maxwell, to achieve high power transfer capability and lower cost. The optimized LCL-S compensated IPT system is also proposed for the railway IPT system to improve the system efficiency. A prototype of the proposed IPT system is developed at an airgap of 5 inches and 85 kHz operating frequency. The prototype has been validated in full power of 5 kW with a DC to DC efficiency of 92.5%, which is the highest efficiency

reported for the railway system. The experimental results validate the feasibility of the IPT system design for rail application.

In addition, the factory manufacturing tolerance effect on the power transfer capability was also investigated. Most of the existing designs have not considered the system inductance variation caused by factory manufacturing tolerance and ambient environment change, which can weaken the power transfer capability of the IPT systems significantly. A 10% coil tolerance can lead to a power reduction of up to 61.3%. To fix this issue, this dissertation proposed a frequency modulated maximum power point tracking (MPPT) method to adjust the inverter frequency to achieve its maximum power point. The simulation results under different circumstances were analyzed. The experimental results show the feasibility of this method in improving the power transfer capability.

ACKNOWLEDGMENTS

First, I would like to express my very great appreciation to my graduate advisor Dr. Tiefu Zhao for the continuous support of my graduate study and research, for his patience, motivation, enthusiasm, and immense knowledge. He guides me to the fantastic world of Power Electronics. I could not complete this journey without his assistance and involvement in every step of my Ph.D. process. I would like to express my deepest appreciation for his support and understanding over the past six years.

I am extremely grateful to my committee members: Dr. Robert Cox, Dr. Michael Mazzola, and Dr. Shen-En Chen, for many precious feedbacks in our discussion to improve my study, and for their encouragement and support in overcoming many obstacles I have been facing throughout my research.

Additionally, this endeavor would not have been possible without the generous support from the Graduate Assistant Support Plan at UNC Charlotte, and N.C. Department of Transportation, who financed my research.

I am also very grateful to all my colleagues and friends, especially Dr. Luocheng Wang, Dr. Yafeng Wang, and Dr. Haichen Liu, for their discussions, helpful feedback, cooperation, moral support, and friendship.

Finally, I must express my profound gratitude to my parents, Mr. Jinglin Xu and Ms. Guiling Chi, my husband, Mr. Yuanming Song, and my two sweet cats, Dexter and Ellie, for providing me with the best spiritual support during my Ph.D. journey and my life in general. This accomplishment would not have been possible without them.

TABLE OF CONTENTS

LIST OF TABLE

LIST OF FIGURES

LIST OF ABBREVIATIONS

A	Ampere
AC	Alternating Current
ADC	Analog to Digital Converter
APT	Acoustic Power Transfer
CO_2	Carbon Dioxide
CPT	Capacitive Power Transfer
DC	Direct Current
DSP	Digital Signal Processor
EMF	Electromagnetic Field
EMI	Electromagnetic Interference
ESR	Equivalent Series Resistance
EV	Electric Vehicle
FEA	Finite Element Analysis
HF	High-frequency
ICNIRP	International Commission on Non-Ionizing Radiation Protection
IPT	Inductive Power Transfer
ISE	Fraunhofer Institute for Solar Energy Systems
J	Joule
KAIST	Korea Advanced Institute for Science and Technology
kW	Killowatt

MMF	Magnetomotive Force
MPPT	Maximum Power Point Tracking
MPT	Microwave Power Transfer
Ms	Millisecond
nF	Nanofarad
OPT	Optical Power Transfer
ORNL	Oak Ridge National Laboratory
PCB	Printed Circuit Board
RF	Radio Frequency
Rx	Receiver
S	Second
SiC	Silicon Carbide
T	Tesla
Tx	Transmitter
V	Volt
VA	Volt-Amp
W	Watt
WPT	Wireless Power Transfer
ZPA	Zero Phase Angle
ZVS	Zero Voltage Switching
Ω	Ohm
μH	Millihenry

CHAPTER 1: INTRODUCTION

1.1 Introduction and Motivation

Human activity in the industrial era is accelerating the speed of global warming caused by greenhouse gas emissions. In order to reduce its impacts on the environment, scientific consensus suggests that the global anthropogenic carbon dioxide (CO_2) emission should decline by about 45% from 2010 levels by 2030, and reach carbon neutrality around 2050 [1]. The United States freight trains have the highest energy demands in rail transport in the world, according to Figure 1-1 (a). Among these different types of energy consumption in Figure 1-1 (b), More than 90% of the freight trains are powered by diesel, which aggressively impacts climate change [2]. These diesel locomotives emit 35 million tonnes of CO_2 each year and produce air pollution that cause about 1000 premature deaths annually, accounting for approximately $6.5 billion in health damages cost per year [3]. Although the current diesel locomotives are installed the catalytic converter to reduce the emissions, the air pollution issue has not been solved from the root causes. In order to

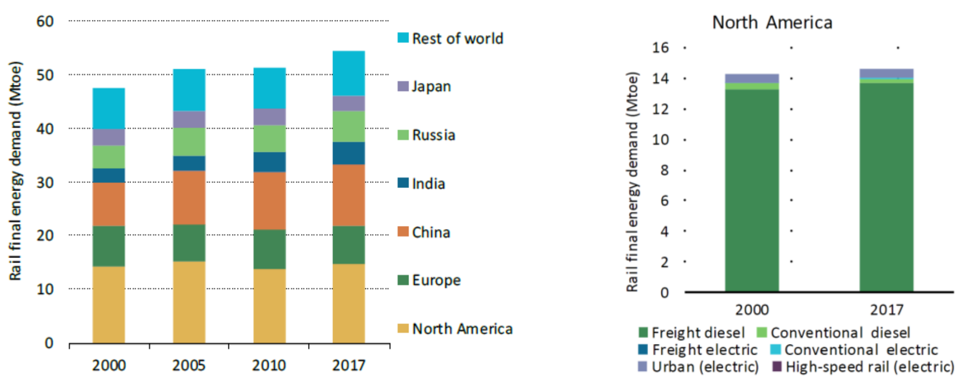

(a) (b)

Figure 1-1 (a) Energy demand in rail transport by region; (b) Source to power the locomotive by type.

achieve zero carbon emissions, a few solutions have been proposed, including developing the hydrogen-powered locomotive and the electric-powered locomotives. Since almost all hydrogen is produced with fossil fuels, which will still cause air pollution, the electrification of the railway system has become a trend in the past decades. The reduced battery price in recent years also accelerated the rail electrification speed.

Therefore, rail electrification has been implemented in many cities at the turn of the 21st century in the US. In addition to being associated with clean energy, the electrified rail is quieter, faster, more reliable, and less expensive in maintenance when compared to the diesel-fueled locomotives. But the cost of electrification infrastructure and equipment is very high (up to $10 million per route mile), which becomes a huge obstacle to realize electrification transformation [31]. Therefore, with the benefits of the lower cost, the higher power efficiency and the reduced environmental impacts, the half-electrified hybrid (diesel-electric) locomotives are more widely accepted and used. However, the current procedure of charging hybrid locomotives is facing many challenges. Different from

(a) (b)

Figure 1-2 (a) A charging locomotive and its charging station; (b) Heavy electrical cable and terminal for charging the locomotives charging the electric vehicle (EV) battery with only a single cord, multiple cords are required to charge a locomotive displayed in Figure 1-2 (a). The power cords shown in Figure 1-2 (b), which are bulky and heavy, have to be moved from the warehouse to the railway and manually connected to the locomotive. The staff responsible for charging the locomotives is exposed to the risk of electric shock while plugging the cables. Besides, the charging is restricted by harsh environmental conditions, such as heavy rain and snowstorm.

In order to overcome these difficulties, wireless power transfer (WPT) technology has been explored as an alternative for wayside power charging of rail locomotives. The charging infrastructure and the onboard system are wirelessly connected via magnetic coupling. The coupled systems have the feature of galvanic isolation, which reduces electrical shock and safety risk. Furthermore, by getting rid of the components associated with the cables, the IPT charging system on locomotives is more flexible and reliable and with better resistance against adverse weather conditions. Different from the IPT technology on the roadway application, the rail tracks provide the locomotives with a fixed route, thus eliminating the lateral misalignment problem, which is very common in EV IPT systems. The IPT infrastructure also has fewer modifications to the conventional railroad compared to the roadway IPT systems which have to rebuild the roads to bury the IPT transmitter systems under the roadway. Finally, the IPT infrastructure can still be utilized after full rail electrification, which can save the overall cost significantly. Thus, IPT technology has huge potential to become the next-generation charging method for hybrid and fully electric locomotives.

1.2 Overview of the Wireless Power Transfer

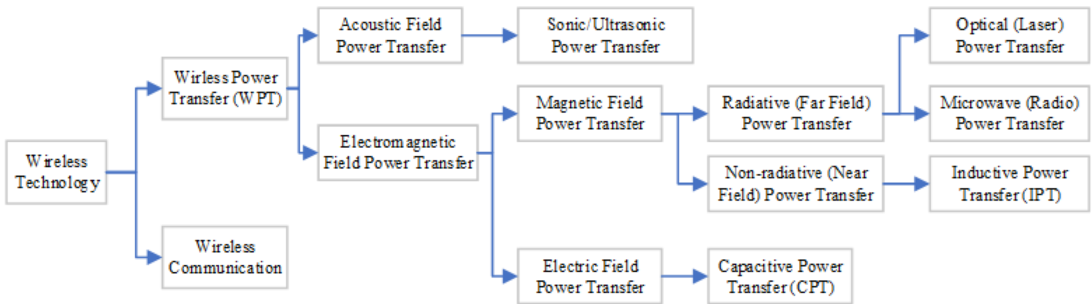

Figure 1-3 Classification of WPT technology

Wireless power transfer (WPT) technology was investigated and developed, as an emerging technology to transfer the power from a transmitter system to a receiver system, without wire connections between them. The concept was first proposed by Nicola Tesla at the turns of 20^{th} century [4], which was to transfer the power wirelessly based on Ampere's law and Faraday's law which describes the interaction between the magnetic field and electric circuits. However, the development of WPT technology was very slow until the end of the 20^{th} century because of the limitations in power electronics, including operating frequency, system efficiency as well as cost. With the emerging development of wide bandgap devices, WPT research is growing rapidly to be applied in implant pacemakers, portable devices, EVs, etc. Figure 1-3 depicts the classification of WPT technology by the category of field, which are acoustic power transfer (APT), optical power transfer (OPT), microwave power transfer (MPT), inductive power transfer (IPT), and capacitive power transfer (CPT) [5]. The characteristics and the applications for each category of WPT will be discussed in this section.

1.2.1 Acoustic Power Transfer

The concept of APT is to use the sound waves to transmit the energy without relying on electrical contact [6]. It is generally used in low power applications such as charging sensors or implant devices with small system dimensions. Since APT does not rely on electromagnetic (EM) field as an energy carrier to transfer the power, APT technology is more applicable for biomedical applications, as well as the power transfer requirement with a metal media, that EM fields are prohibited. However, the main challenges of the APT are the reflections and the resulting spatial resonances issues, which limit the system efficiency. Based on the record in [6], the efficiency of APT systems could generally reach approximately 50%. The loss model is complicated, therefore difficult to modelized to describe all the loss effects according to the examined literature.

1.2.2 Optical Power Transfer

The concept of OPT is based on the principle of the photoelectric effect, which allows energy to be transferred over a long distance up to several kilometers. The common media of OPT is laser because of its efficient atmospheric propagation window as well as its ability to deliver a large amount of power to a small aperture. Though the long-distance power transfer capability brings benefits and flexibility to the power transmission, the drawbacks of OPT, such as low efficiency (20% or less), potential safety issues to human beings and animals, as well as the line-of-sight requirement of transmitters and receivers, makes the OPT application be generally used in aero-based power transfer, such as unmanned aerial vehicles, robots, and orbiting satellites [7].

1.2.3 Microwave Power Transfer

MPT is also a far-field WPT technology that transfers the energy via microwave (GHz-order radio wave). It requires the rectifying antenna or rectenna, a radio frequency (RF) receiver that consists of an antenna and rectifying circuit with a diode or CMOS, to converter the RF power to the direct current for energy harvesting purposes. MPT has been wildly used in telecommunications, however, there are many challenges of WPT application for the high power transmission purpose. The power density of a high-power WPT system is low. For example, it needs a 3.4 m × 7.2 m rectenna array to receive 30 kW power by WPT [8]. The efficiency of the system is mostly less than 50%. Besides, the radiation of the microwave is not human-friendly, which also limits the application of WPT. Nowadays, power transmission by microwaves is applied in aircrafts and satellites.

1.2.4 Capacitive Power Transfer

CPT transfers the power from anode metal plates to cathode metal plates via the electric field. The power transfer capability of CPT relies on the coupling capacitance between the transmitter and receiver. The low permittivity of air limits the coupling capacitance, which requires the compensation circuit to provide higher voltages for generating stronger electric fields to transfer power. Benefits from low eddy current losses and low cost, CPT has been used in many low-power applications, such as integrated circuits, biomedical devices, LED lighting, and mobile device charging [5]. In recent years, CPT could transfer several kilowatts power, which became a candidate for EV charging applications. However, the efficiency and the power density of CPT in high power application is the main concern. The transmission distance is also the primary constraint limiting the CPT to be applied in a mid-airgap charging.

1.2.5 Inductive Power Transfer

IPT is used the magnetic field to transfer the power wirelessly. The power could be transferred via magnetic coupling from a small to medium range airgap distance. It provides galvanic isolation between the transmitter and receiver systems. IPT is suitable for systems rated from several watts to several hundred kilowatts, with an efficiency of around 90%. Nowadays, IPT technology has been commercialized in many low-power systems, such as implant device charging and mobile device charging. IPT is also relatively mature in EV application, because it could achieve high efficiency, high power rating, high power density, mid-airgap requirement, as well as safety requirements. However, there are still some challenges of IPT, especially applying it to some high-power systems. The main disadvantage of IPT is that it leads to a significant eddy current loss in its ambient metals during the energy transmission. The electromagnetic interference (EMI) might cause safety issues for humans, which needs to be taken into consideration while the rated power of the IPT system increases to several kilowatts.

1.3 Development of IPT for Railway Applications

Since Nicola Tesla proposed the wireless power transfer concept, IPT technology has been investigated extensively. However, the development of IPT technology was very slow until the end of the 20th century because of the limitations in power electronics, including operating frequency, system efficiency as well as cost. With the emerging development of wide bandgap devices, IPT research is growing rapidly to achieve a higher output power, higher efficiency, and lower cost. During the past decades, numerous research institutes have proposed different IPT systems and demonstrated several prototypes for EV application [9] – [16]. Witricity developed a 3.3kW wireless charging system with an efficiency of 90% at 18cm airgap in 2013 [17] and an 11kW wireless charging system with 91 – 94% efficiency in 2016 [18], respectively. IPT technology has presented a 100kW wireless charging solution for electric buses [19]. The team from Fraunhofer Institute for Solar Energy Systems (ISE) demonstrated a 22kW bidirectional charging system with a pulse density modulation (PDM) method to achieve a system efficiency of 97.4% [20]. Oak Ridge National Laboratory (ORNL) proposed a 120kW IPT system with 96.9% DC-DC efficiency in a 5 inches airgap in 2018 [21]. Table 1-1 displays some designs and prototypes of the IPT system in industry and academia for EV application, which have a trend for high power and high efficiency. Therefore, IPT technology is relatively mature and commercialized in EV applications.

Table 1-1 IPT system designs for EV applications

Name	**Year**	**Air gap**	**Power**	**Efficiency**	**References**
KAIST	2009	1 cm	3 kW	80%	[22]
KAIST	2009	17 cm	60 kW	72%	[23]
KAIST	2010	20 cm	15 kW/pick up	83%	[24]
KAIST	2010	20 cm	27 kW	80%	[25]
Bombardier	2013		200 kW		[26]
Witricity	2013	18 cm	3.7 kW	90%	[17]
Toshiba	2014	16 cm	7 kW		[27]
BOSCH	2015		7 kW	86%	[28]
Fraunhofer ISE	2015	13 cm	22 kW	97.40%	[20]
Witricity	2016	9 – 28 cm	11 kW	91 - 93%	[18]
INTIS	2016	11 cm	30 kW		[29]
ETH	2016	16 cm	50 kW	95.80%	[30]
Toshiba	2017	10 cm	44 kW		[31]
ORNL	2018	15 cm	50 kW	95%	[32]
ORNL	2018	5 inches	120 kW	96.90%	[21]
WAVE	2019		500 kW		[33]
Zhejiang University	2020	16 cm	50 kW	95.20%	[34]
Momentum dynamics	2021		450 kW		[35]
ORNL	2021		200 kW	98.30%	[36]
IPT technology			100 kW		[19]

For railway applications, however, only a few projects of IPT system design have been reported. Bombardier PRIMOVE developed a 250-kW IPT system for trams [15]. Korea Advanced Institute for Science and Technology (KAIST) proposed and optimized several coupler designs and IPT system designs up to 100kW for rail applications from 2010 to 2015 [37] – [44]. They also implemented a 1-MW dynamic IPT system with an efficiency of 82.7% [43]. In 2020, KAIST improved the system efficiency to 90.8% at 12.7kW, with an airgap of 23 cm [48]. For all of the KAIST designs, the cores are mostly composed of core plates. These designs lead to high core volumes in the system, which increase the core material costs. Although the I-type coupler design and S-type coupler design can receive more magnetic flux on the receiver sides, which improves the power transfer capability, they also cause power fluctuations when the misalignment occurs or during the dynamic charging. The system efficiencies are less than 90% at their full power operating conditions. Southwest Jiaotong University team developed a dual transmitter and receiver design for the railway application which has been validated at 1.5kW [45]. The power transfer capability is improved by the dual transmitters enhancing the magnetic field, and the dual receivers capturing more magnetic field. However, the crossing coupling between two coils will decrease the efficiency and transmitted power. The decoupled transformers are required to be added to the circuit to reduce this impact. In 2021, Harbin Institute of Technology team proposed a three-phase IPT system for the railway application, which has been validated at 5kW with an efficiency of 82.7%. The coil distribution for the I-type cores reduces the power fluctuations during the dynamic charging compared to the single-phase coils. Whereas, the core volumes are still high that increases the core material cost. Table 1-2 indicates the current research works of wireless charging development for railway applications. The detailed challenges for railway applications are discussed in the next section.

Table 1-2 IPT system designs for railway applications

Name	Year	Air gap	Power	Efficiency	Reference
KAIST	2010	20cm	27kW	74%	[37]
KAIST	2011	20cm	60kW	83%	[38]
KAIST	2012		100kW		[39]
KAIST	2012	20cm	79.5kW	81.70%	[40]
KAIST	2013	20cm		91%	[41]
KAIST	2014	26cm	100kW	80%	[42]
KAIST	2015	5cm	1MW	82.70%	[43]
KAIST	2015	20cm	22kW	87%	[44]
Southwest jiaotong University	2017	12cm	1.5kW		[45]
UNCC	2018	5cm	1.1kW		[46]
Pathumwan institute of technology	2019		17.5kW	69.14%	[47]
KAIST	2020	23cm	12.7kW	85%	[48]
Harbin Institute of Technology	2020	30cm	5kW	82.70%	[49]

1.4 Challenges of IPT on Railway Applications

The application of the IPT system for charging locomotives is still facing a lot of challenges. One of the key technical challenges is that the general coupler design for EVs, such as the circular pad, DD coupler [5], and DDQ coupler [50], cannot meet the design considerations for wireless train charging. An IPT system for charging locomotives needs a higher power rating and a more flexible charging space to ensure the parking spot tolerance will not severely affect the power transfer capability. A modular design is more suitable for the railway system to be extended easily to achieve a high power rating and compensate for the parking spot tolerance. Furthermore, coupler designs for the railway application, such as S-type coupler [44] and I-type coupler [37], have the null position. It significantly reduces the power transfer capability during misalignment and leads to power fluctuations during dynamic charging. The ideal IPT system should have high compatibility to dynamically charge the locomotives when they are entering or leaving the stations and to stationarily charge the trains when they are parked in the station. The coupler design must be compatible with both dynamic and stationary charging. Besides, the current coupler designs mostly have high core volumes, which increases the core material cost. The coupler design for the railway system should be cost-effective and maintain its power transfer capability. The IPT electrical system needs to be co-designed with the magnetic couplers to maximize the performance for high efficiency and better system stability. The system is also required to eliminate the communication between the transmitter and receiver to simplify the system and keep it robustly. The control method should be implemented not only to control the output power but also to have a cost-effective way to maximize the power transfer capability.

1.5 Overview of the Proposed Research

In order to fill the gaps and challenges of IPT system for the railway application, a W-I shaped coupler is proposed, which has a relatively higher coupling coefficient and a significantly lower core volume to reduce the core material cost and maintain the power transfer capability. The modular design is easy to be extended for both static and dynamic charging. Finite element analysis (FEA) by ANSYS Maxwell has been conducted to optimize the W-I core design to fulfill a higher coupling coefficient. The W-I shaped coupler was also compared with the current coupler designs for the railway application in terms of coupling coefficient, core material cost, and misalignment tolerance.

According to the characteristics and constraints of the railway system, a modular LCL-S IPT system design for charging locomotives was also optimized in the dissertation. The compensation circuit has been co-designed with the proposed W-I coupler to minimize the number of passive components used in the system, which improves the system efficiency. The LCL-S compensation network could also eliminate the communication between the transmitter and receiver side, and maintain the system stability during the misalignment conditions. The co-simulation was conducted to analyze the losses in the magnetic system and electrical system. A prototype of the W-I coupler based IPT system is developed to validate the design. The prototype has been tested at 5 kW with a DC-DC efficiency of 92.5%, which is the highest IPT system efficiency reported for railway applications.

Besides, most of the existing IPT system designs have not considered the system inductance variation caused by factory manufacturing tolerance and ambient environment change, which can weaken the power transfer capability of the IPT systems significantly. In this dissertation, the effects of the inductance variation on the power transfer capability of IPT systems were investigated. A 10% coil tolerance can lead to a power reduction of up to 61.3%. To fill this gap, this dissertation proposed a frequency modulated MPPT method to adjust the inverter frequency to achieve its maximum power point. The simulation results under different circumstances were analyzed. The experimental results show the feasibility of this method in improving the power transfer capability.

1.6 Organization of the Dissertation

Chapter 1 introduces the importance and motivation of implementing the wireless charging system for railway applications. The challenges of the railway IPT system are discussed. Chapter 2 reviewed the state-of-the-art IPT technology in terms of coupler design, compensation circuit design, controller design, as well as the electromagnetic interference (EMI) standard for high-power applications. The detailed technical gaps and challenges are discussed in this chapter. Chapter 3 introduces the proposed W-I shaped coupler design in detail. The FEA results and the prototype development are also demonstrated. In Chapter 4, the proposed LCL-S compensated IPT system design for the railway system is introduced. The detailed simulation results and experimental results are presented in this chapter. Then, Chapter 5 illustrated the inductor variation impact on the power transfer capability. A frequency modulated MPPT method was proposed to fix the resonant frequency and improve the transferrable power. The simulation and experimental results are shown in this section. Chapter 6 summarized the research works and author’s contributions, as well as the future works to complete and optimize the proposed system designs.

CHAPTER 2: LITERATURE REVIEW

2.1 Introduction

A regular IPT charging system shown in Figure 2-1 consists of two electrical systems without wire connections. Two electrical systems, the transmitter system (primary side) and receiver system (secondary side), are coupled magnetically and transfer the power via the magnetic field. Two physical laws are applied to the inductive charging procedure: Ampere's Law and Faraday's Law. Ampere's Law states that the changing electric current generates the changing magnetic field. Faraday's Law states that the changing magnetic field produces the induced voltage in the circuits. The DC power supply is converted to a high-frequency switching power and injected into the transmitter coil via a DC/AC inverter. The power is transferred wirelessly via the coupled coils with a certain airgap distance. During this procedure, energy was transduced from electrical energy to magnetic energy by Ampere's Law in the transmitter and then transduced back to electrical energy based on Faraday's Law in the receiver. The high-frequency induced voltage on the receiver side is converted to a DC voltage by a rectifier. A DC/DC converter might be used to control the power flow from the receiver to the load. The compensation circuits on the transmitter and receiver sides are resonant with the transmitter and receiver coils, respectively, which are aimed to reduce the VA rating as well as maximize the power transfer capability.

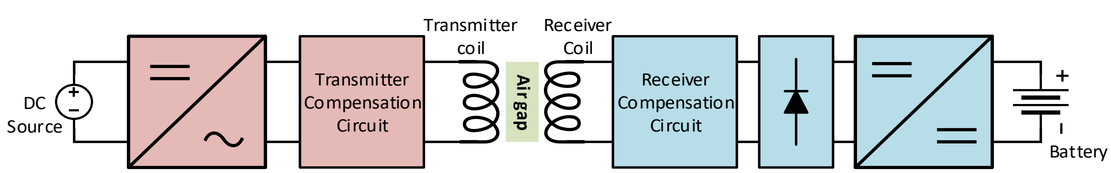

Figure 2-1 IPT charging system diagram

[51] proposed a method to derive the output power in an IPT system. Assumed the L_s and L_p are the self-inductance of the transmitter coil and receiver coil with a mutual inductance M. For a track current (current in transmitter coil) I_1 operating at an angular frequency ω, the induced voltage on the receiver is,

$$V_{oc} = j\omega M I_1 \tag{2.1}$$

If the receiver side is shorted, the short current is,

$$I_{sc} = \frac{V_{oc}}{j\omega L_p} = \frac{M I_1}{L_p} \tag{2.2}$$

The product of (2.1) and (2.2) is the maximum VA rating for the receiver called P_{su}. The maximum power P_{out} that the system can transfer is,

$$P_{out} = P_{su} \cdot Q_2 = \omega \frac{M^2}{L_p} I_2^2 Q_2 \tag{2.3}$$

where Q_2 is the quality factor of the secondary side that is compensated by the receiver compensation circuit. According to equation (2.3), the output power is positively proportional to ω, M, I_1, or Q_2. Since the IPT system is sensitive to the frequency, increasing the frequency could increase the power but also have to change the designed values of the compensation circuit, which is not feasible in a designed IPT system. A higher frequency will also cause EMI safety issues in a high-power operating condition. Increasing the mutual inductance will not require any variation of the designed IPT parameters, which is the best solution to increasing the power. The mutual inductance, however, is constrained by the coupler size, coupler material, configuration of the coil, etc. Increasing the track current will increase the magnetomotive force (MMF) on the primary side coil to improve the output power while decreasing the system efficiency by more power consumption on the primary side wires. Increasing Q_2 of the secondary side current is another solution, but the VA rating on the receiver circuit is increased and the bandwidth is narrowed. These factors make the design of the IPT systems complicated. In order to design an IPT system for a locomotive, the IPT design considerations need to be taken in four aspects,

1) Coupler design;
2) Compensation circuit and system design;
3) Controller design;
4) Electromagnetic interference (EMI) standard investigation.

In this chapter, these design aspects for the railway applications are investigated. The effects of different design considerations and how these factors affect the system performance are analyzed and discussed.

2.2 Coupler

The coupler is one of the most critical parts of an IPT system. It is comprised of the transmitter core and coil as well as the receiver core and coil. The design of a coupler determines the coupling coefficient k of the system [52]. For a higher k value, more power could be transferred to the secondary side with the same track current. A good coupler design will also have a higher misalignment tolerance. The k value could be improved by adding the ferrite cores in the transmitter and receiver coil. However, the ferrite cores with high permeability increase the cost of an IPT system significantly. Thus, there is a trade-off between the coupler cost and the coupling coefficient of the couplers. Many coupler designs are proposed in recent years to improve the power transfer capability.

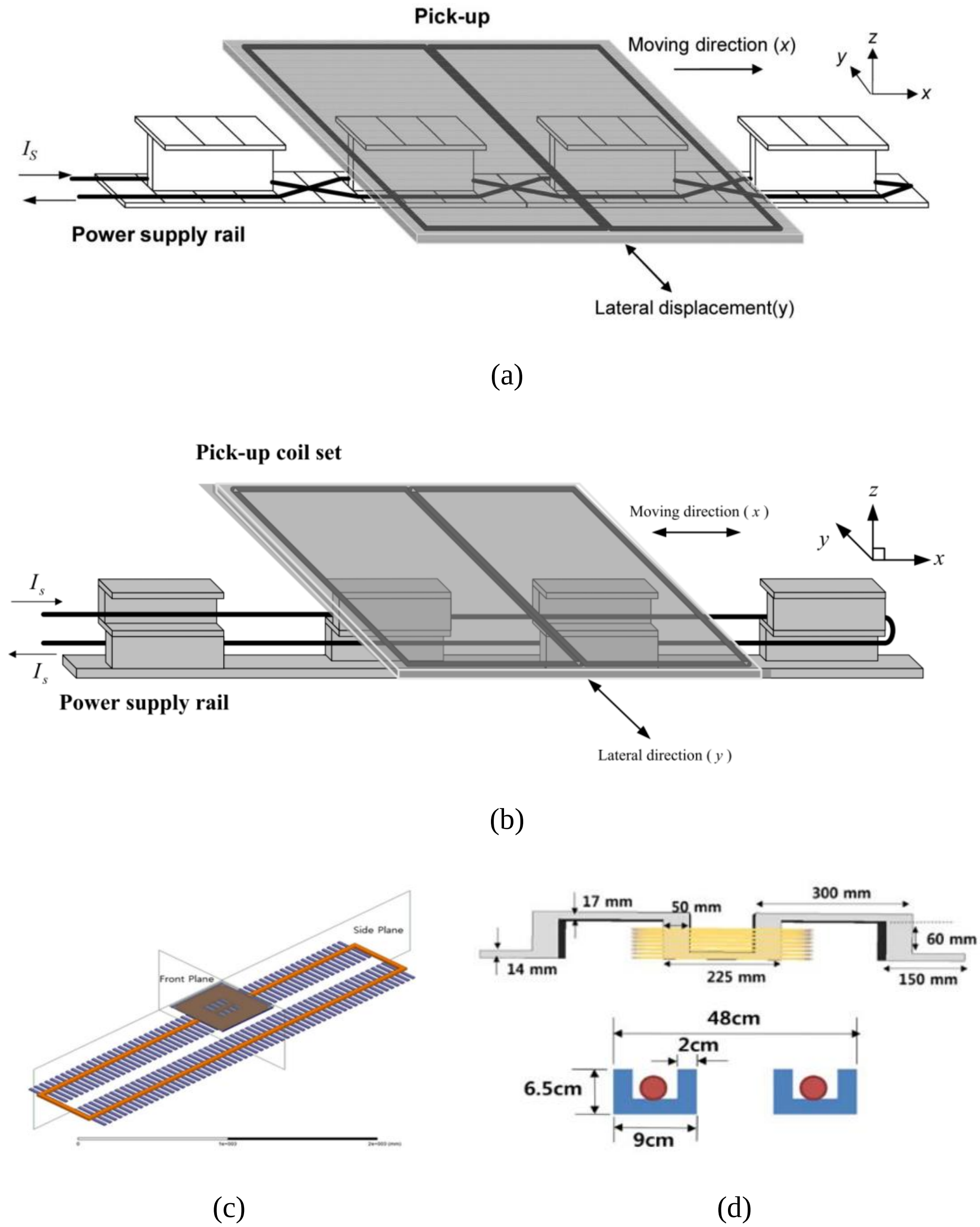

Figure 2-2 Coupler designs from KAIST team: (a) I type coupler; (b) S type coupler; (c) Rectangular coupler; (d) 1-MW project coupler.

A research team from KAIST works on the wireless charging for locomotives since 2010 [37] – [44], [48]. Most of their designs selected the operating frequency at 20 kHz, which made it possible to achieve the highest power efficiency as well as a high output power with a large air gap. As shown in Figure 2-2, four types of coil designs were developed for the railway system. In 2011, the I-type coupler displayed in Figure 2-2 (a) was developed for a 60kW IPT system with an airgap of 20 cm. The system could achieve a frequency of 83%. The S-type coupler shown in Figure 2-2 (b) was proposed in 2015 for a 22kW IPT system. The narrow-width design is more compact and has less leakage magnetic field. For both I-type and S-type designs, the flux directions at neighborhood poles are in opposite directions. These core designs canceled the electromagnetic field (EMF) by neighborhood poles and reduced the EMF for pedestrians around the power supply. A large lateral displacement is also allowed in this design. However, these two designs all have a null position when the pickup coils are located between two I-type or S-type core units. This null position will cancel the magnetic field across the receiver and reduce the power transfer capability, making the designs not applicable for static charging. During the dynamic charging, the system will also have a large power fluctuation that weakens the transferable power as well as affects the control system stability. Besides, the core designs consist of many core plates, which have a high core volume and leads to an expensive core material cost. The KAIST research team also developed a 1-MW IPT system for a high-speed train with two U-type cores on the transmitter and an E-shape core on the receivers shown in Figure 2-2 (d). This design reduced the misalignment problem as well as reduced the magnetic field above the pickup with E shape core. Figure 2-2 (c) demonstrates the coupler design proposed in 2020 for the railway application. The system was validated at 12.6kW with a 23 cm airgap and an 85% maximum efficiency. Both of these two designs have a much longer transmitter coil than the receiver, which is more

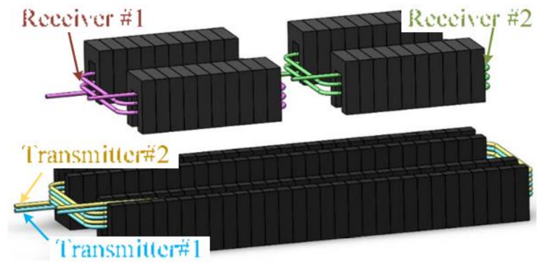

Figure 2-3 Coupler design from Southwest Jiaotong University

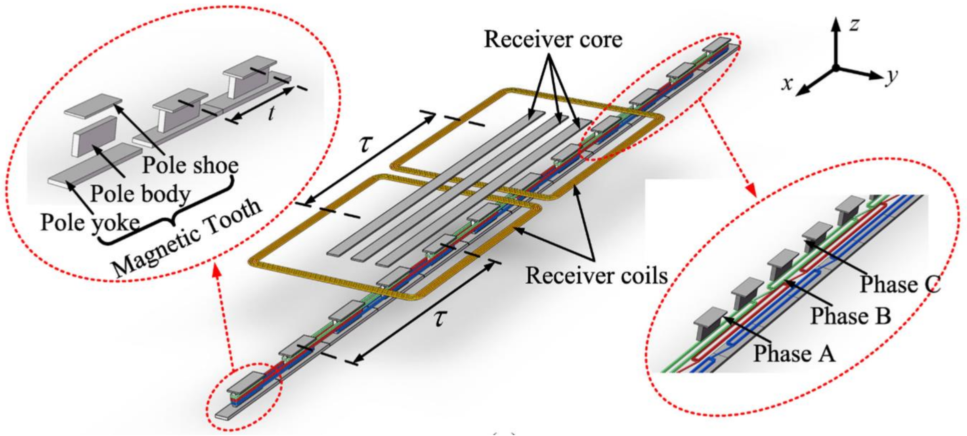

Figure 2-4 Coupler design from Harbin Institute of Technology

suitable for dynamic charging. If the trains stop at a station for static charging. Most of the magnetic flux will be wasted or generate extra losses due to the small size of the receiver.

Southwest Jiaotong University team proposed a dual transmitter and receiver coupler design for wireless locomotive charging in 2017. Figure 2-3 displays their coupler design. The system operated at 20kHz with a 1.5kW output power. The dual transmitter could enhance the magnetic field, and the dual receivers could capture more magnetic fields. Thus, the power transfer capability will be improved in this design. However, the crossing coupling between two coils will decrease the efficiency and transmitted power. The decoupled transformers are required to reduce this impact. The system efficiency is not evaluated in their paper.

Figure 2-4 presents a three-phase coupler design for the railway system from Harbin Institute of Technology team. The operating frequency is also 20kHz with an airgap of 30 cm. The system has been operated at 5 kW with an efficiency of 82.7%. The coil distribution reduces the fluctuation of the output power compared with a single phase I type transmitter. But the core volume is still high, which reflects the core material cost.

2.3 Compensation Circuit and System Design

In a loosely coupled IPT system (coupling coefficient $k < 0.5$), such as the battery charging for EVs or locomotives, the leakage inductance on the primary and secondary side is relatively high compared with conventional transformers. Hence, the leakage inductance is required to be compensated for providing more power to the receiver as well as reducing the VA rating of the source. The requirements of the compensation circuits are concluded as follows [53] – [58],

1) maximize the power transfer capability;

2) minimize the VA rating on the source side and load side;

3) provide a constant current or constant voltage output;

4) avoid the bifurcation phenomena [54];

5) increase the system efficiency.

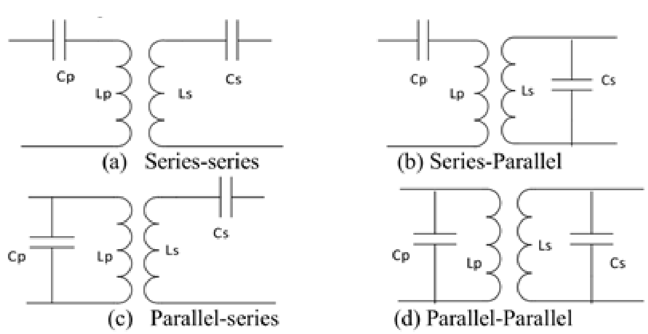

Figure 2-5 Basic compensated topologies for IPT system

Figure 2-5 shows the four basic compensated topologies SS, SP, PS and PP of IPT system, where the first S or P stands for the series or parallel compensation on the transmitter side and the second S or P represents the series or parallel compensation on the receiver side [54]. S compensation on the primary side provides a large VA rating at the input side while the P compensation on the primary side has a low VA rating at the power supply. The compensated Cp is independent of the load in S compensated primary, but Cp in P compensated primary is a function of the load. In series compensated secondary side, the load is required to be small for maximum the power transfer while the load should be large in parallel compensated secondary side. The series-series topology is the easiest topology to design an IPT system because the system can work at a frequency independent of the coupling factor and load. However, the transmitter coil current might have the over current issue during a low couping coefficient condition. Therefore, the communication between the transmitter and receiver is required to control the track current. The parallel-parallel topology is also a good choice for the design because of the low VA rating at the transmitter side as well as the pure current source characteristics on the receiver side - which is more suitable for battery charging [55]. However, the change of the coupling coefficient will affect the resonant frequency because of the equivalent capacitance change, which increases the complexity of the controller design. Besides the basic compensation topologies, the LCL compensation [58] [59], LCC compensation [55] – [57], [61] also become competitive compensation topologies applied in the IPT system because of its better performance and characteristics. [60] proposed an analysis method to design the compensation circuit in order to achieve constant voltage or constant current output.

2.4 Controller

The operating frequency at or near the secondary resonant frequency is a logical choice in most applications because the maximum power transfer capability can be achieved. Furthermore, it is also desired that the output voltage and current of the power supply be in phase, in order to minimize the VA rating of the power supply. In order to achieve the operating frequency range, both the primary controller and secondary controller need to be implemented in the IPT system. The primary controller is responsible for the primary current magnitude control in order to achieve maximum power transfer capability. The secondary controller is responsible for the power flow regulation by means of a switched-mode controller within the secondary pickup for power flow control [53].

There are two methods for frequency control: Fixed frequency control and variable frequency control. Fixed frequency control is easier to operate. However, if the load and coupling factor have large and variable ranges, the power supply will need a higher VA rating for the same power transfer. On the other hand, the variable frequency controller operates at the primary ringing frequency and the operational frequency (ZPA frequency of the load impedance) will shift away from the nominal resonant frequency because of the variations in load and the degree of coupling between the primary and secondary coils. This results in a loss of power transfer capability if the frequency shift is too large and may also result in a loss of frequency stability and controllability [53].

2.5 EMI Standard

The IPT system transfers the power via high-frequency magnetic fields, which cannot be shielded. In loosely coupled IPT systems, the leakage flux is relatively high and should be constrained to meet the requirements of the standards for human safety.

There are four standards regarding EMI in the low-frequency range. The first standard is the ICNIRP 1998 / ICNIRP 2010 [63]. The International Commission on Non-Ionizing Radiation Protection (ICNIRP) provides scientific advice and guidance on the health and environmental effects of non-ionizing radiation (NIR) to protect people and the environment from detrimental NIR exposure. In ICNIRP 2010, the average magnetic field exposed limit is 27 uT for general public exposure, while the limit is 100 uT for occupational exposure. IEEE Std. C95.1 2005 provides recommendations to protect against harmful effects in human beings exposed to electromagnetic fields in the frequency range from 3 kHz to 300 GHz are provided in this standard. The limit is 205 uT for general public exposure, while the limit is 615 uT for occupational exposure [64]. Another standard is IEC61980 [65]. In this standard, IEC 61980 1:2015 covers general requirements for Electric Vehicle (EV) Wireless Power Transfer (WPT) systems, including general background and definitions for example efficiency, electrical safety, Electromagnetic Compatibility (EMC), protection from electromagnetic field (EMF) and so on. IEC 61980 2:2019 contains the requirements for the communication between EV and WPT systems when connected to the supply network. IEC 61980 2:2019 covers specific requirements for EV magnetic field wireless power transfer (MF WPT) systems. The last is FCC rules, which require Wireless power transfer devices operating at frequencies above 9 kHz are intentional radiators and are subject to either Part 15 and/or Part 18 of the FCC rules [56]. In order to promise safety, the standard with the lowest value is selected which is the standard of ICNIRP 2010.

The measurement point for EV application has been determined in J2954 [66], a guidance for the stationary applications of WPT system for EV. The measurement point is

0.8m away from the center of the WPT system. This point is also the edge of the train carriage. For the railway application, however, there is no specific standard or rules for the WPT system [75]. There is a standard IEC 62957 about magnetic field levels with respect to human exposure. This standard determines the measurement points for both inside and outside of the locomotives. The measurement points outside the locomotive are 0.3m to the surface, with different measuring heights of 0.5m, 1.5m, and 2.5m. For safety purposes, the 0.8m measurement point was selected to measure the EMF.

CHAPTER 3: PROPOSED WI COUPLER DESIGN FOR THE RAILWAY SYSTEM

3.1 Introduction

Figure 3-1 depicts a conceptual IPT system for charging a train wirelessly [68]. The IPT system for the railway application contains a transmitter infrastructure embedded between the tracks and an on-board receiver system located on the underbelly of the locomotive. The DC power is converted to a high-frequency AC power and injected into the transmitter coil via an inverter. The power is transferred wirelessly via the coupled coils with a certain airgap distance. During this procedure, energy was transduced from electrical energy to magnetic energy by Ampere's Law in the transmitter and then transduced back to electrical energy based on Faraday's Law in the receiver. The compensation circuits on the transmitter and receiver sides are resonant with the transmitter and receiver coils, respectively, which are aimed to reduce the VA rating as well as maximize the power transfer capability. The high-frequency induced voltage on the receiver side is converted

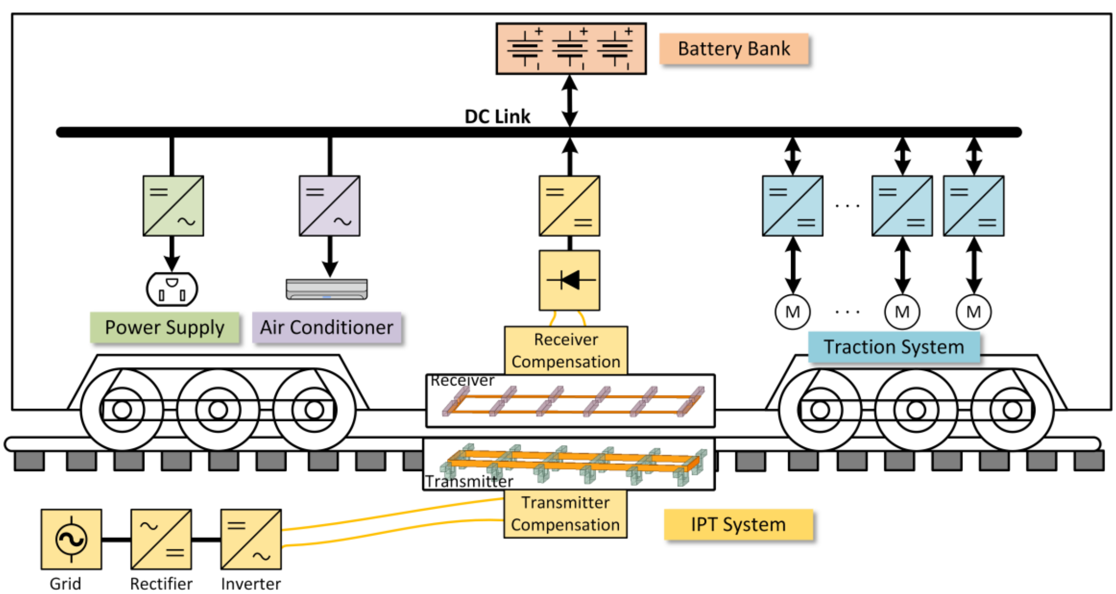

Figure 3-1 Conceptual diagram of wireless train charging application

to a DC voltage by a rectifier. A DC/DC converter might be used to control the power flow from the receiver to the batteries and loads. Therefore, the IPT design needs to consider both magnetic design (coupler) and electrical design (compensation circuits and converters).

The shape and size of the coupler are constrained by the track gauge and the chassis size of the locomotives. Since the tracks are made of iron, the edge of the coupler should not be too close to the tracks, which can lead to additional magnetic losses by generating stranded eddy current within the tracks. Although the coupler length has considerable design flexibility because the standard length of a locomotive is 20m long, a longer coupler would increase the cost considerably as well as increase the difficulty for the installation of a single-piece coupler system. The minimum required distance from the bottom of the locomotive to the top of the tracks defines the airgap between the coupler for the locomotives, which leads to the IPT system becoming a loosely coupled system.

The power transfer capability is directly affected by the *k* value according to Equation (2.3). Thus, achieving a higher coupling coefficient *k* becomes one of the main objectives to improve the power transfer capability of a loosely coupled IPT system. Towards this goal, core material with a higher permeability is also required to achieve a higher *k* value. As a wireless charging system for railway applications, the coupler design should be capable of both stationary and dynamic charging. Currently proposed couplers for train applications such as the I-type coupler designs have relatively high *k* values, but they also require precise positions on which the power transfer capability is fully realized. Since it is difficult to park the locomotive at an accurate spot during the stationary, it is

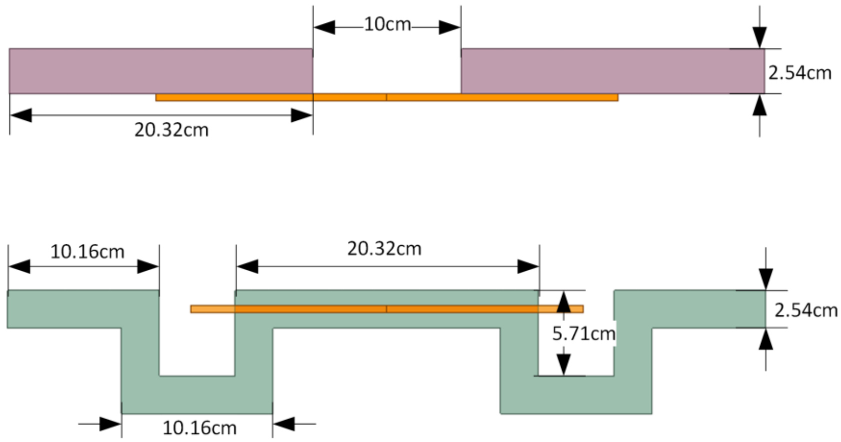

(a)

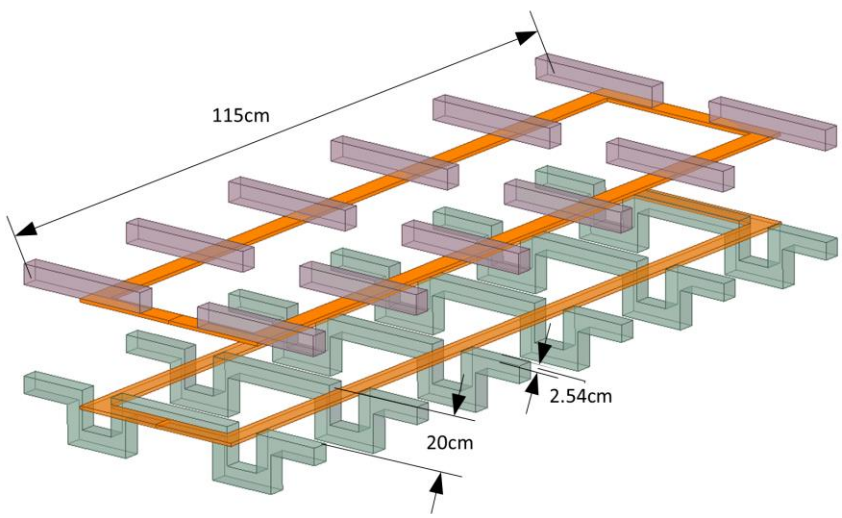

(b)

Figure 3-2 Dimensional information of the proposed W-I shaped coupler (a) Overview; (b) Front view.

inevitable for a locomotive to be parked at a null position with almost zero power transfer capability. The null position of I-type designs significantly reduces the transferable energy of the IPT system during stationary charging.

Based on the constraints and requirements discussed above for the wireless locomotive charging, a W-I shape coupler depicted in Figure 3-2 is proposed for the IPT system for railway application. The coupler consists of a W-shaped transmitter (Tx) core and two I-shaped receiver (Rx) cores. The core material is Ferroxcube 3C90 which has a relative permeability of 2300. The airgap of the coupler is designed to be 5 inches (12.7cm). The shape and size of the coupler, as well as the position of the coils, were optimized via ANSYS Maxwell to achieve the highest coupling coefficient *k* to increase the output power transfer capability. The coupler was designed to be a modular discrete distributed system along the tracks, which reduces the cost of the cores and increases the feasibility of installation.the tracks, which reduces the cost of the cores and increases the feasibility of installation.

3.2 Coupler Optimization

Figure 3-3 shows the magnetic circuit of the proposed coupler design for optimizing the coupler geometry. The flux received by the receiver Φ_{Rx} and the leakage flux from the transmitter Φ_{Lkg} can be represented as follows,

$$\Phi_{Rx} = \frac{2 \cdot mmf}{R_{gap} + R_{Rx} + R_{air} + R_{Tx}} \tag{3.1}$$

$$\Phi_{Lkg} = \frac{2 \cdot mmf}{R_{Lkg} + R_{Tx}} \tag{3.2}$$

where mmf is the magnetomotive force generated in the transmitter coils, and R_{Tx}, R_{Rx}, R_{gap}, R_{air}, and R_{Lkg} are the magnetic reluctance of the transmitter cores, receiver cores, airgap, and air. The coupling coefficient k reflects the ratio of received flux Φ_{Rx} to the total flux Φ_{Rx}+Φ_{Lkg} [46]. Based on Equation (3.1) and (3.2), the *k* value can be expressed as follow,

$$k = \frac{\Phi_{Rx}}{\Phi_{Rx} + \Phi_{Lkg}} = \frac{1}{1 + \frac{R_{gap} + R_{air} + R_{Tx} + R_{Rx}}{R_{Lkg} + R_{Tx}}} \tag{3.3}$$

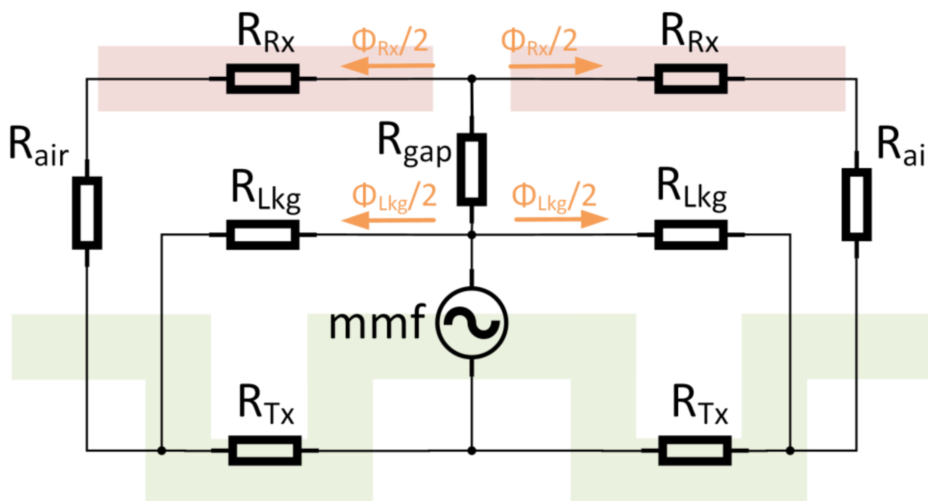

Figure 3-3 Magnetic equivalent circuit of the proposed W-I coupler.

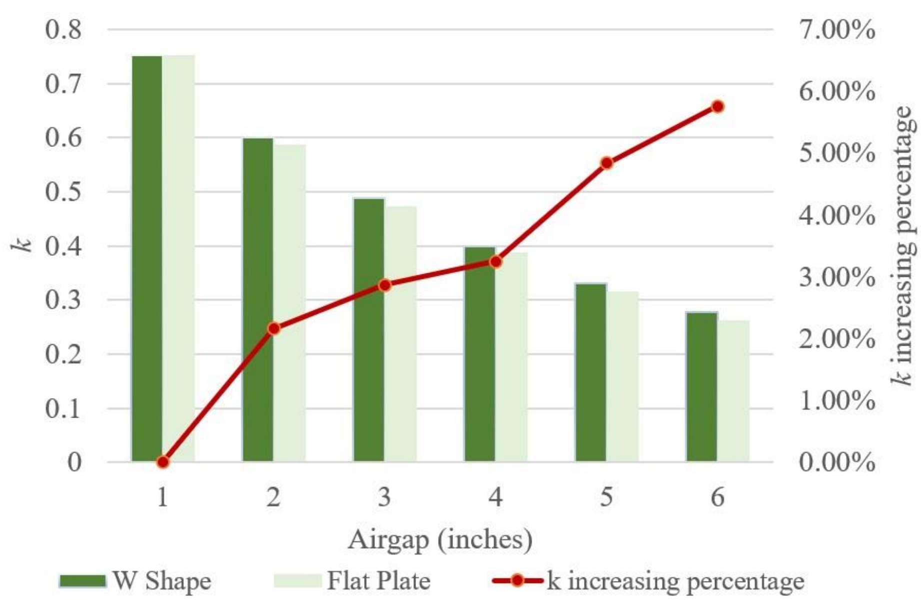

Figure 3-4 Increasing percentage of k value by varying airgap distances.

The geometry of the coupler is one of the critical factors for improving the coupling coefficient *k*. By implementing the W shape on the transmitter side, R_{Lkg} near the transmitter increases by introducing more air reluctance in the magnetic loop compared with the regular flat plate core with the same length and thickness. Thus, the k value is improved with the increase of R_{Lkg} according to Equation (3.3). Figure 3-4 displays the FEA results that compared the performance between a W slots core shown in Figure 3-2 (a) and a flat plate core with the same length, width, and thickness. The figure demonstrates the k value improving percentage of the W shape transmitter in different airgap distances. When the airgap is smaller, R_{gap} and R_{air} are sharply decreased to make Φ_{Rx} increase significantly. Φ_{Lkg} is reduced and takes a much smaller portion of the total magnetic flux generated from the transmitter. So the coupling coefficient between the transmitter and receiver is lifted by reducing the airgap distance. In this situation, though the W shape core reduces the Φ_{Lkg}, the impact on k improvement is negligible due to the analysis above. By increasing the airgap distance, Φ_{Lkg} takes a higher portion in the total generated magnetic flux. The effect of shape optimization is more obvious in improving the k value. Therefore, the W shape transmitter can improve the power transfer capability by increasing the k value in a loosely coupled system. The coupling coefficient is enhanced by 4.8% while the designed airgap is 5 inches, which can improve the power transfer capability of an IPT system by 10% based on Equation (3.1). On the receiver side, the shape of the receiver affects R_{Rx} value. The I-type receiver design in Figure 3-2 (a) provides the shortest magnetic path compared with other shape designs, thereby having a lowest R_{Rx}. The k value is enhanced according to Equation (3.3) by implementing the I-type receiver. Consequently, the coupler is optimized to the W-I shape to achieve a higher coupling coefficient in a loosely coupled IPT system.

Then, the dimensional optimization was conducted on the design parameters shown in Figure 3-5, which include:

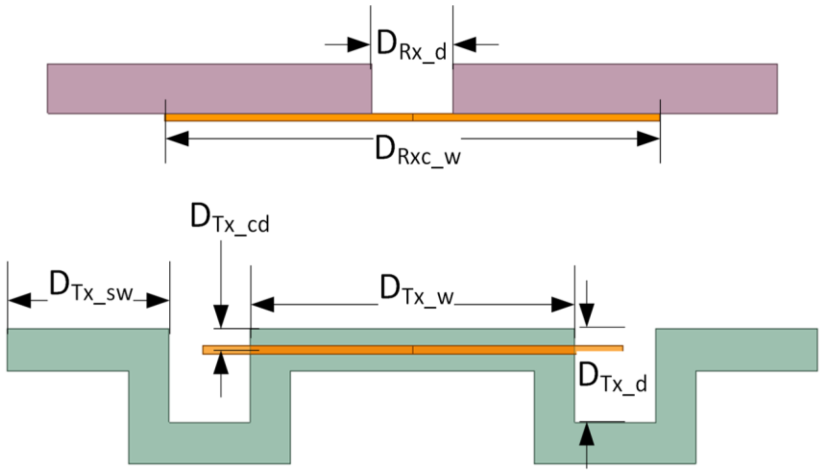

Figure 3-5 Design parameters of proposed W-I coupler

- length of transmitter flanges D_{Tx_sw};
- depth of transmitter U-shape slots D_{Tx_d};
- distance between the two I-shape receiver cores D_{Rx_d};
- width of receiver coil D_{Rxc_w};
- position of transmitter coil D_{Tx_cd}.

Since k is determined by the radius of both Tx and Rx coils, the width of Tx coil, also known as D_{Tx_w}, is first determined as 20.32 cm. By varying the design parameters, the FEA results of k are displayed in Figure 3-6. Figure 3-6 (a) and Figure 3-6 (b) show the optimization for the length of transmitter flanges and the depth of transmitter U-shape slots, respectively. According to the FEA simulation, the longer D_{Tx_sw} and D_{Tx_d} are, the higher the coupling coefficient k would become. However, the increase of D_{Tx_sw} and D_{Tx_d} will become less effective to increase k and, at the same time, result in more eddy current loss in the tracks and increase the cost of the coupler. By taking these factors into consideration,

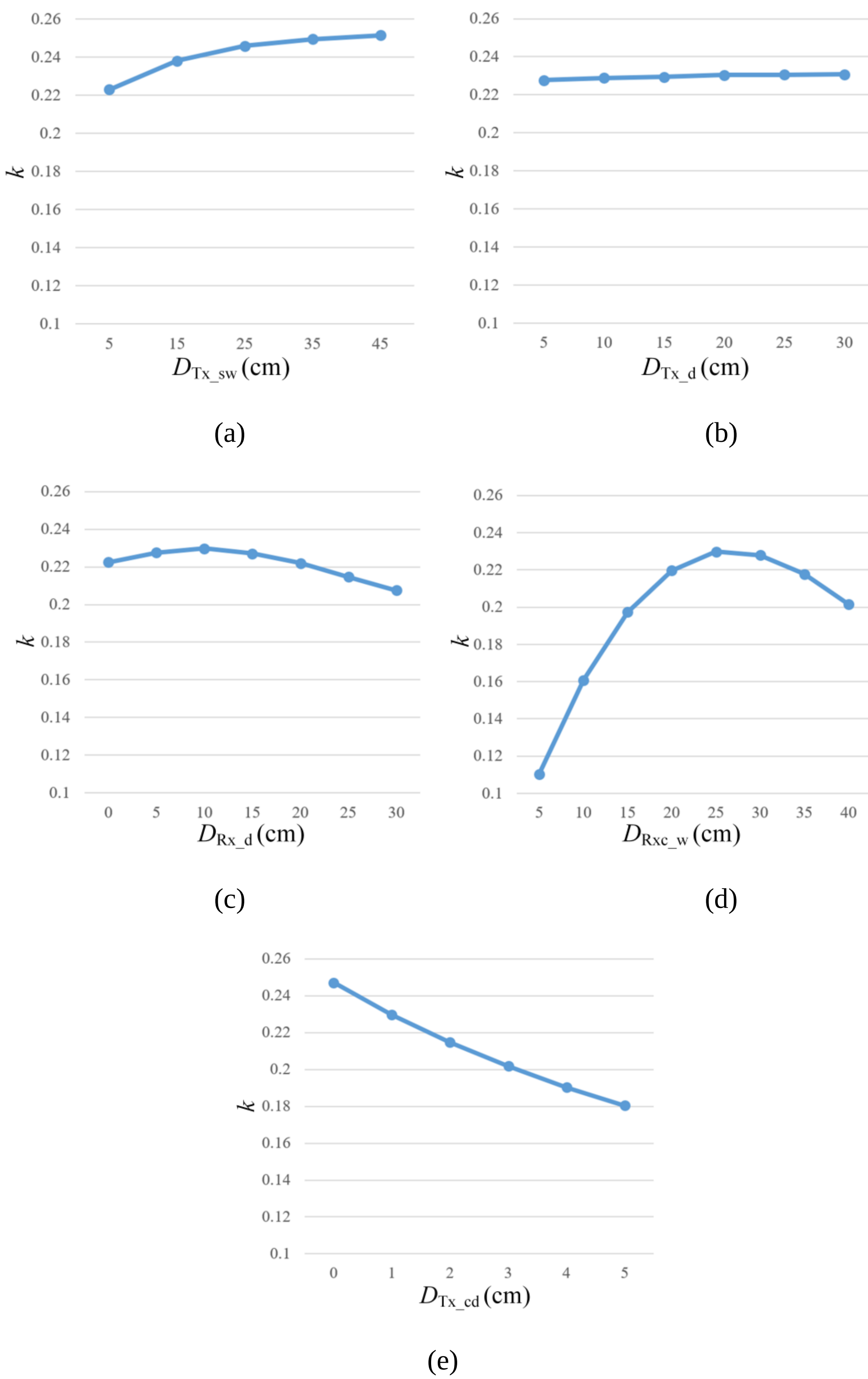

Figure 3-6 FEA results of design parameters. (a) D_{Tx_sw} vs. k; (b) D_{Tx_sw} vs k; (c) D_{Rx_d} vs k; (d) D_{Rx_d} vs k; (e) D_{Rx_d} vs k.

D_{Tx_sw} and D_{Tx_d} values are determined and are shown in Figure 3-2. Figure 3-6 (c) and Figure 3-6 (d) demonstrate the k value variation by modulating the distance between two I-shape receiver cores D_{Rx_d} and the width of receiver coil D_{Rxc_w}. The k achieves the maximum value with D_{Rx_d} = 10 cm and D_{Rxc_w} = 25 cm. The relationship between the position of the transmitter coil and the k value is depicted in Figure 3-6 (e). By lifting D_{Tx_cd} from the bottom to the top of the U-shape slots, the k value improved from 0.180 to 0.247, which increases the k value by 37.2%. Thus, the ideal position of the transmitter coil is on the top edge of the U-shape slots. However, installing and fixing of Tx coil will become difficult for hardware development. Therefore, the final design of the W-I coupler includes the thickness of Tx coil support into consideration, which determined the D_{Tx_cd} to be 1 cm.

The relative permeability μ_r is also an important core materials parameter, which affects the power coupling coefficient and power transfer capability. Higher μ_r will increase the coupling coefficient of the coupler, but the price will also be more expensive at the same time. After the shape and size of the coupler have been determined, the relative permeability is also a critical parameter to ensure the system has a high transferable power as well as a lower cost. The FEA was implemented to vary the μ_r from 1 (same as air) to 2500 to observe the coupling coefficient change. Figure 3-7 displays the coupling coefficient as well as the output power changes while the relative permeability is increasing. According to Figure 3-7, a higher coupling coefficient will improve the output power level of the IPT system. The coupling coefficient increases rapidly while the relative permeability is less than 2000, which prompts a significant increase of the output power. The increasing rate of k is less than 5%, while the relative permeability is more than 2000. Thus, the relative permeability around 2000 is a reasonable selection for the core material.

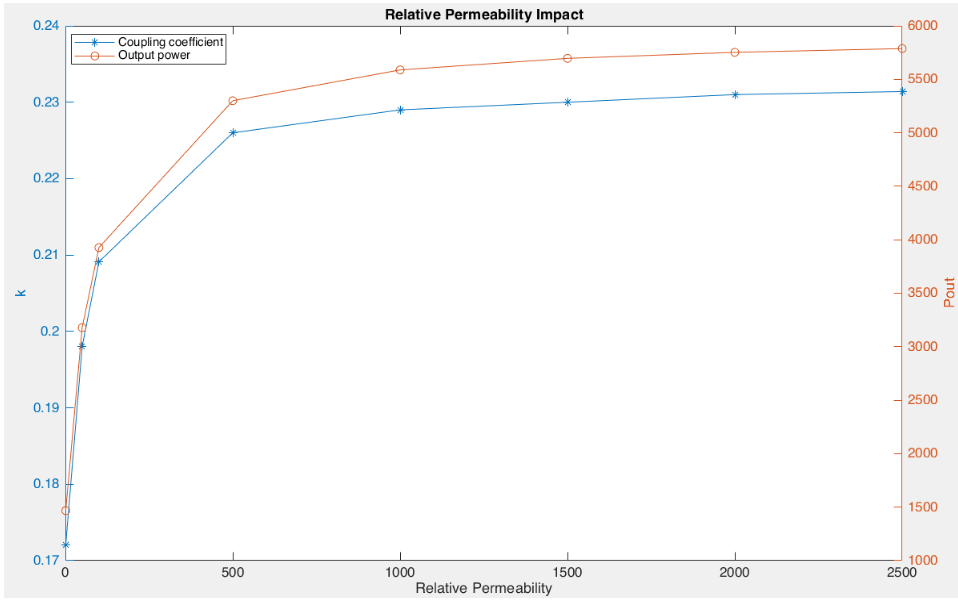

Figure 3-7 Relative permeability impact on power transfer capability

The core material is finally determined to be Ferroxcube 3C90 with a relative permeability of 2300.

3.3 FEA Results

The FEA results of the optimized W-I coupler are demonstrated in Figure 3-8 and Table 3-1. The simulated airgap is 5 inches. and the couple coefficient *k* is 0.236 based on the FEA results.

Table 3-1 FEA Results

Parameter	Symbol	Value
Tx self-inductance	L_p	70 uH
Rx self-inductance	L_s	175 uH
Mutual Inductance	M	26.1 uH
Coupling coefficient	k	0.236
Airgap	D_{Air}	5 in

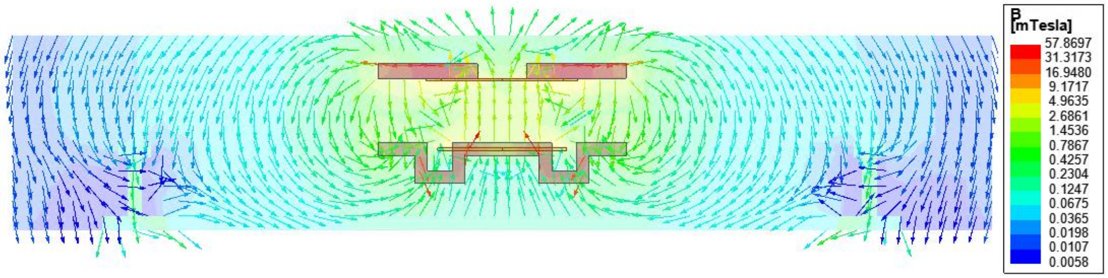

(a)

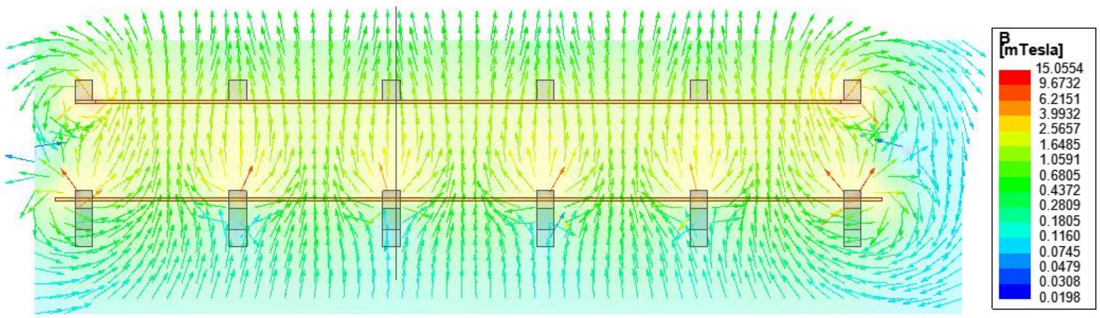

(b)

Figure 3-8 Magnetic flux density overlay of the W-I core. (a) Front view; (b) Side view.

3.3 Core Design Evaluation

In order to evaluate the proposed W-I coupler, FEA was also conducted for different coupler designs for the railway application, including aligned I-type coupler [67] in Figure 3-9 (a), paralleled I-type coupler [46] in Figure 3-9 (b), U-U design coupler [43] in Figure 3-9 (c), and the propose W-I coupler in Figure 3-9 (d). The comparison focuses on the coupling coefficient and the volume of cores in the transmitter and receiver, which indicate the power transfer capability and the cost of the core material. The coupler designs are all constrained to be one meter in length. The simulated *k* values, the core volumes, and the estimated core material cost are displayed in Figure 3-10. The cost of the core material

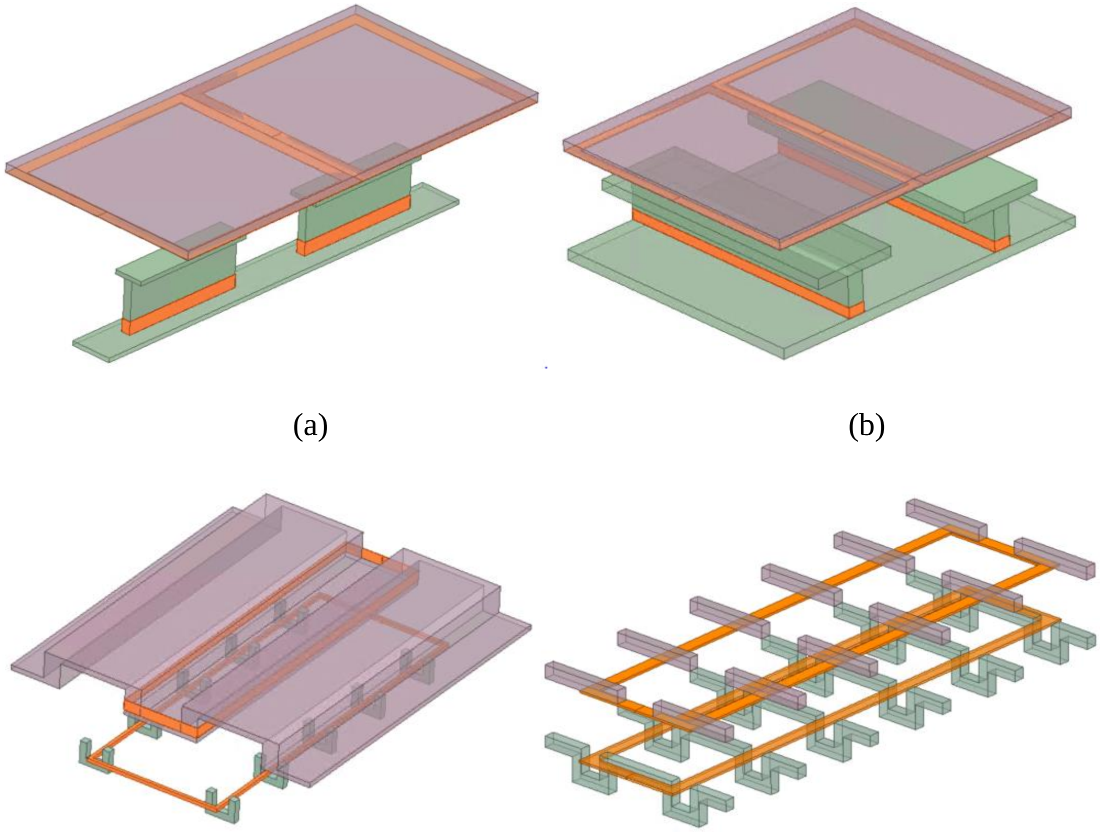

(a) (b)

(c) (d)

Figure 3-9 Four types of coupler designs: (a) aligned I-type, (b) paralleled I-type, (c) U-U design, (d) proposed W-I coupler.

is estimated to be \$0.1515/cm^3 based on the marketing investigation. According to the results in Figure 3-11, the paralleled I-type coupler shown in Figure 3-9 (b) has the highest *k* value of 0.345. However, the volume of the cores is also the highest among the four types of coupler designs, which means it has the highest cost of the core material. The core material cost of the W-I shaped coupler reduces by 93.2%, but the coupling coefficient is only reduced by 31.6%, compared to the paralleled I-type coupler. The coupler design in Figure 3-11 (a) and Figure 3-11 (c) have higher core volumes as well as lower *k* values wh-

Figure 3-10 Power transfer capability and core material cost comparison.

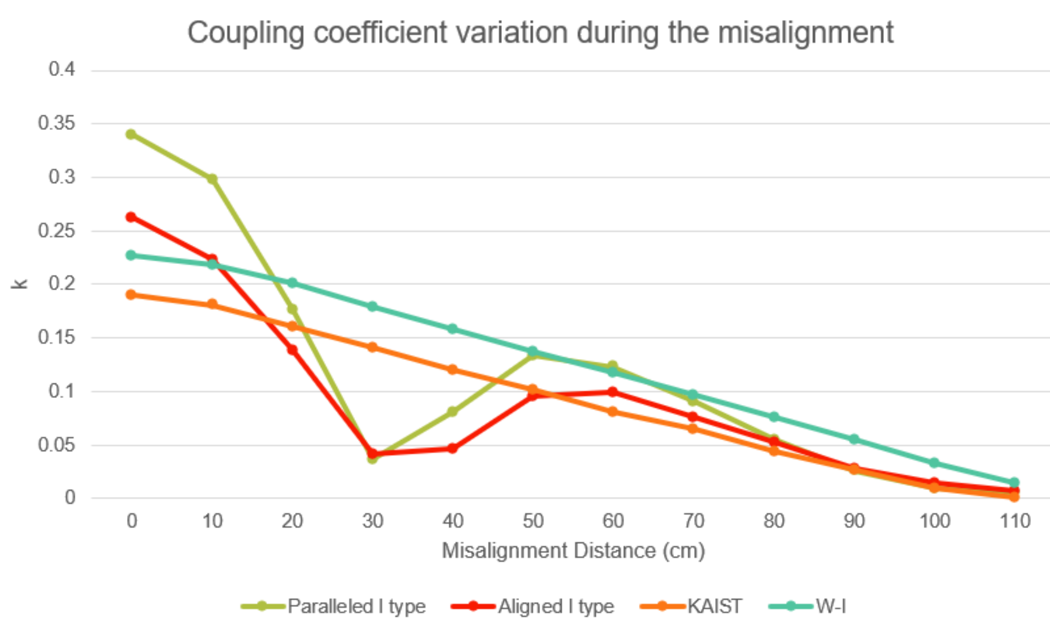

Figure 3-11 Misalignment tolerance comparison.

en compared to the proposed W-I coupler shown in Figure 3-11 (d). The W-I coupler has great advantages in both power transfer capability and core material cost. Thus, the W-I coupler is the coupler design of choice with relatively higher power transfer capability and cost-saving characteristics.

The misalignment tolerance for four types of coupler designs is also analyzed. The locomotives have two tracks to guide their route, so they don’t have the lateral misalignment. This section only assesses the longitudinal misalignment that might occur for the railway IPT systems. The coupling coefficient change is simulated by ANSYS Maxwell from the aligned position to a misalignment distance of 110 cm. The FEA results are shown in Figure 3-11. Two I-type designs have higher coupling coefficients when the misalignment is less than 10 cm. Due to the existence of the null position, however, the coupling coefficient reduces significantly when the misalignment distance is between 20 cm and 50 cm. If the coupler is used for dynamic charging, these two designs also have an output power fluctuation during the charging that impact the total transferable power. The W-I coupler provides the highest power transfer capability in this misalignment range. When the misalignment is more than 50 cm, the power transfer capability of the two I-type coupler designs is slightly recovered to the same level as W-I shaped coupler. Therefore, the W-I shaped coupler has a more stable performance when a misalignment distance is in the IPT system. It can even provide a higher power transfer capability compared to the bipolar coupler designs in their null positions.

3.4 Core Loss Evaluation

The FEA of core loss is conducted to estimate the proportion of the core loss to the total losses. Since the core material has been determined to be Ferroxcube 3C90, the B-H

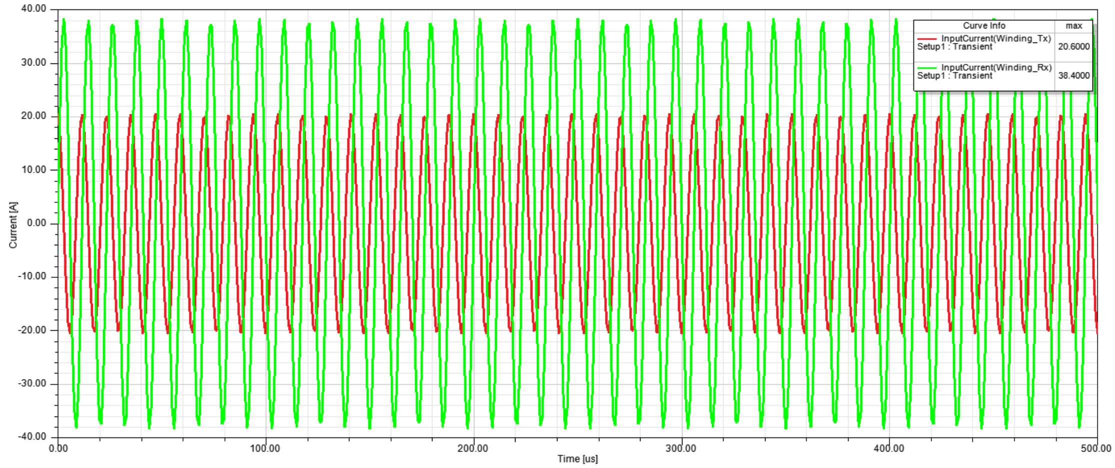

(a)

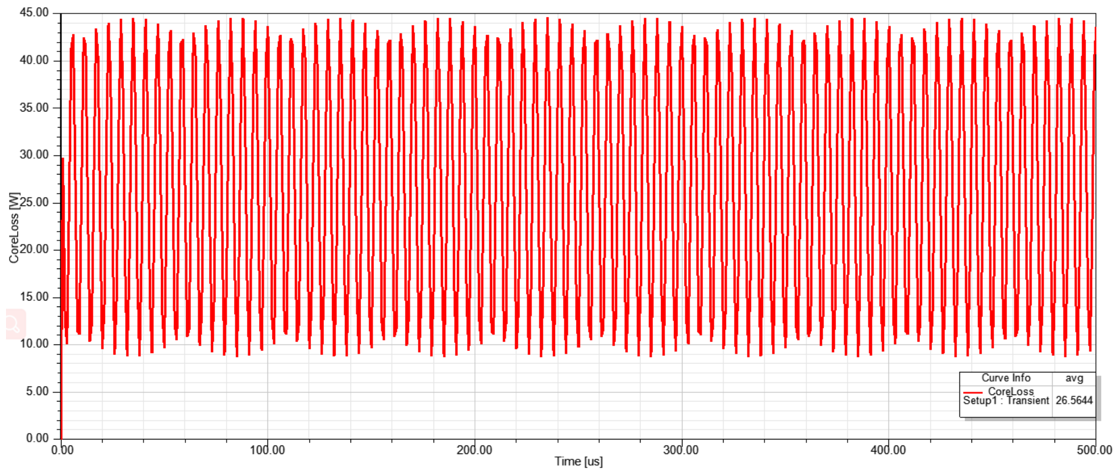

(b)

Figure 3-12 (a) Excitation current in transmitter coil (Red) and receiver coil (Green); (b) Simulation results of core loss at 5kW operating condition.

curve and B-P curve of the material could be imported to ANSYS Maxwell for the core loss evaluation. The electrical circuit is also co-simulated for providing the excitation current and induced voltage to the coupler coils. More detail about the circuit design is presented in Chapter 4. The simulation condition is that the W-I coupler operates at 650V input voltage and 5kW output power. The operating frequency is 85kHz. The simulation results of the transmitter and receiver coil current, as well as the core loss, are shown in Figure 3-12. The transmitter coil peak current is 20.8 A, while the receiver coil peak current is 38.4 A. The core loss is 26.56 W at 5kW operating condition, which takes only 0.53% of the output power. The core loss of the designed W-I coupler accounts for a small proportion of the 5kW testbed.

3.5 Prototype Development

Figure 3-13 demonstrates the prototype of the W-I shaped coupler. The core material is Ferroxcube 3C90, with a relative permeability of 2300. The coupler coils are the 38/1500 Liz wires, which could alleviate the skin effect in high operating frequencies to reduce the AC losses. It has five turns on the transmitter side, and eight turns on the receiver side. The self-inductance and the mutual inductances are measured by the LCR meter to validate the design. Table 3-2 displays the comparison between the simulation results and the testing results. The measured coupling coefficient is 0.215 at 5 inches airgap.

In conclusion, the proposed W-I shaped coupler is an optimized design for the railway application. It has a high power transfer capability with a low core material cost according to its discrete core design. The coupler has a good misalignment tolerance for

Table 3-2 W-I coupler parameters

Parameter	**Symbol**	**Theoretical Value**	**Measured Value**
Tx self-inductance	L_p	70 μH	70.4 μH
Rx self-inductance	L_s	175 μH	174.6 μH
Mutual Inductance	M	26.1 μH	23.8 μH
Coupling coefficient	k	0.236	0.215
Airgap	D_{Air}	5 inches	5 inches

(a)

(b)

Figure 3-13 Prototype of the proposed W-I shaped coupler.(a) transmitter; (b) receiver.

stationary charging and less power fluctuation for dynamic charging. The core loss only accounts for a tiny proportion of the output power, which will improve the system efficiency. The modular design is easy for extension and applicable for both static and dynamic charging.

CHAPTER 4: IPT SYSTEM DESIGN FOR THE RAILWAY SYSTEM

4.1 Introduction

In contrast to tightly coupled systems, loosely coupled IPT systems require the compensation circuits on both transmitter and receiver sides to reduce the VA rating on the source and load sides and maximize the power transfer capability. Different combinations of the compensation topologies have been introduced in Chapter 2. As stated earlier, there is some degree of difficulty parking a locomotive at a precise charging position. The coupling coefficient may vary each time while the locomotive is parked on the top of the transmitter. Hence, a constant track current irrelative to the coupling coefficient is desired to provide a constant magnetomotive force to the receiver and ensure the stability of the power transfer process. The constant track current is also beneficial for dynamic charging to simplify the control system. There have been many compensation topology designs such as LCC-S and double side LCC to fulfill these requirements. The second capacitor in series with the transmitter coil increases the design flexibility. However, these designs will also increase the number of passive components to increase the conduction loss as well as affect the system efficiency. In order to simplify the compensation circuit to reduce the component and keep its benefits, an optimized LCL-S compensation topology shown in

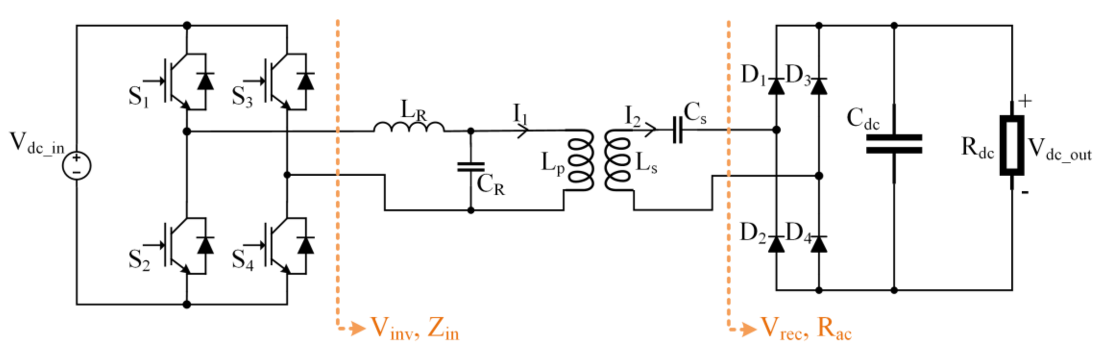

Figure 4-1 Proposed LCL-S compensated IPT system for railway application.

Figure 4-1 is proposed for the IPT system to charge the locomotive wirelessly. The co-design for electrical circuits and magnetic coupler is implemented to ensure the compensation circuit has a minimum number of passive components, which can maintain the design requirements and improve the system performance. The LCL-S compensation circuit also provides a constant track current which will not be affected by the misalignment and load variation. Thus, the communication between the transmitter and receiver side could be eliminated. This design will simplify the control system.

This chapter aims to design a 5kW modular IPT system for locomotive wireless charging. The circuit modeling and analysis have been discussed in detail in this chapter. The experimental results of the designed IPT system for locomotive charging are also demonstrated in the chapter.

4.2 Circuit Modeling

Figure 4-1 shows the equivalent circuit of the LCL-S compensation circuit. This topology removes the capacitor in series with the transmitter coil in the LCC-S topology to reduce the number of passive components in the circuit and lower the conduction loss in the compensation circuit. Due to the compensation circuits filtering the high-order harmonics, only the fundamental frequency, which is also the designed resonant frequency,

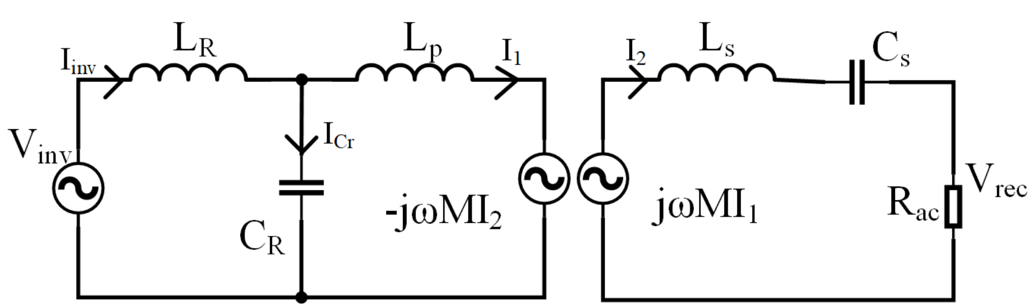

Figure 4-2 LCL-S compensation circuit equivalent circuit.

is analyzed. According to the Fourier analysis, the inverter output voltage V_{inv} and the equivalent resistance R_{ac} can be derived respectively as,

$$V_{inv} = \frac{2\sqrt{2}}{\pi} V_{dc\_in} \tag{4.1}$$

$$R_{ac} = \frac{8}{\pi^2} R_{dc} \tag{4.2}$$

where V_{dc_in} is the input DC voltage and R_{dc} is the load resistance. To minimize the volt-ampere (VA) rating, the compensation circuits are required to be operated at the resonant frequency [54]. Therefore, the design constraints of the LCL-S compensation circuit are,

$$\begin{cases} \omega L_R = \dfrac{1}{\omega C_R} \\ L_R = L_p \\ \omega L_s = \dfrac{1}{\omega C_s} \end{cases} \tag{4.3}$$

where L_p and L_s are the self-inductances of transmitter and receiver. By analyzing the equivalent circuit in Figure 4-2 via Kirchhoff's Voltage Law (KVL), the track current I_1 and rectifier voltage V_{rec} are derived as follows,

(4.4)

$$V_{rec} = j\omega M I_1 \tag{4.5}$$

where L_R and C_R are the resonant inductance and resonant capacitor on the transmitter side. According to Equation (4.4), the track current only depends on the input voltage V_{inv}, switching frequency ω, and resonant parameters in the transmitter, like L_R and C_R. The track current can be kept constant while the coupling coefficient k and the load R_{ac} vary. Based on Equation (4.5), the LCL-S compensation circuit also provides a load-independent output voltage. Besides, by the frequency domain analysis of the inverter output voltage and current, the high-frequency inverter is capable of achieving zero voltage switching (ZVS) while the system operates at the designed resonant frequency.

4.3 Parameters Optimization

In order to optimize the LCL-S IPT system to achieve high efficiency, the designed transmitter inductor L_p and receiver inductors L_s effects, as well as the airgap (k value) effects on the IPT system efficiency were analyzed. The losses in the inverter and rectifier are minimal and could be negligible owing to the soft-switching and the diode feature, respectively. Thus, the losses in the compensation circuit are mainly discussed. The equivalent circuit of the LCL-S compensation circuit is depicted in Figure 4-3. According to the KVL analysis, the circuit matrix and the current in each path could be derived as,

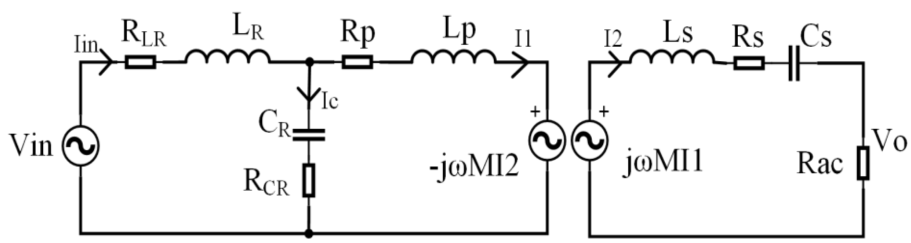

Figure 4-3 Proposed LCL-S compensated IPT system for railway application.

$$\begin{bmatrix} V_{in} \\ 0 \\ 0 \end{bmatrix} = \begin{bmatrix} R_{LR} + R_{CR} & -j\omega L_R - R_{CR} & 0 \\ 0 & -j\omega M & R_s + R_{ac} \\ R_{CR} + j\omega L_R & -Rp - R_{CR} & j\omega M \end{bmatrix} \cdot \begin{bmatrix} I_{in} \\ I_1 \\ I_2 \end{bmatrix} \tag{4.6}$$

The input current I_{in}, track current I_1, and the output current I_2 could be derived from Equation (4.6),

$$I_1 = \frac{V_{in}\left(R_{ac} + R_s\right)\left(R_{CR} + j\omega L_R\right)}{Z_1} \tag{4.7}$$

$$I_2 = \frac{j\omega M\, V_{in}\,(R_{CR} + j\omega L_R)}{Z_1} \tag{4.8}$$

$$I_{in} = \frac{V_{in}\,(M^2\omega^2 + R_{ac}R_{CR} + R_{ac}R_p + R_{CR}R_s + R_pR_s)}{Z_1} \tag{4.9}$$

where,

$$\begin{aligned} Z_1 = {} & \omega^2 L_R{}^2 (R_{ac} + R_s) + \omega^2 M^2 (R_{CR} + R_{LR}) + R_{ac}R_{CR}R_{LR} \\ & + R_{ac}R_{CR}R_p + R_{ac}R_{LR}R_p + R_{CR}R_{LR}R_s + R_{CR}R_pR_s \\ & + R_{LR}R_pR_s - 2j\omega L_R R_{CR}(R_s + R_{ac}) \end{aligned} \tag{4.10}$$

In the equations above, I_{inv} is the inverter output current, I_1 is the transmitter coil current (track current), I_2 is the receiver coil current, R_{LR}, R_p, R_s, and R_{CR} are the ESRs of inductors and capacitors in the compensation circuit. Therefore, the output power P_{out} and the system efficiency η could be obtained as,

$$P_{out} = I_2{}^2 R_{ac} \tag{4.11}$$

$$\eta = \frac{I_2{}^2 R_{ac}}{I_{in}{}^2 R_{LR} + (I_{in} - I_1)^2 R_{CR} + I_1{}^2 R_p + I_2{}^2 R_s + I_2{}^2 R_{ac}} \tag{4.12}$$

The variation of R_{ac} represents the change of operating point, as well as determines the transferable power and efficiency of the IPT system. The target of the optimized operating point is to work at the 5kW rated output power with relatively high efficiency by considering the parameter optimization and the capacitor selection. The nominal values of L_p, L_s, and k are determined from the coupler design in Table 3-1. Based on the constraints of the compensation circuit in Equation (4.3), the compensation capacitor values could be derived while analyzing the L_p and L_s changes. By substituting Equation (4.7), (4.8), and (4.9) into Equation (4.11) and (4.12), the output power and efficiency variation can be depicted as shown in Figure 4-4. The marked points in each curve exhibit the maximum

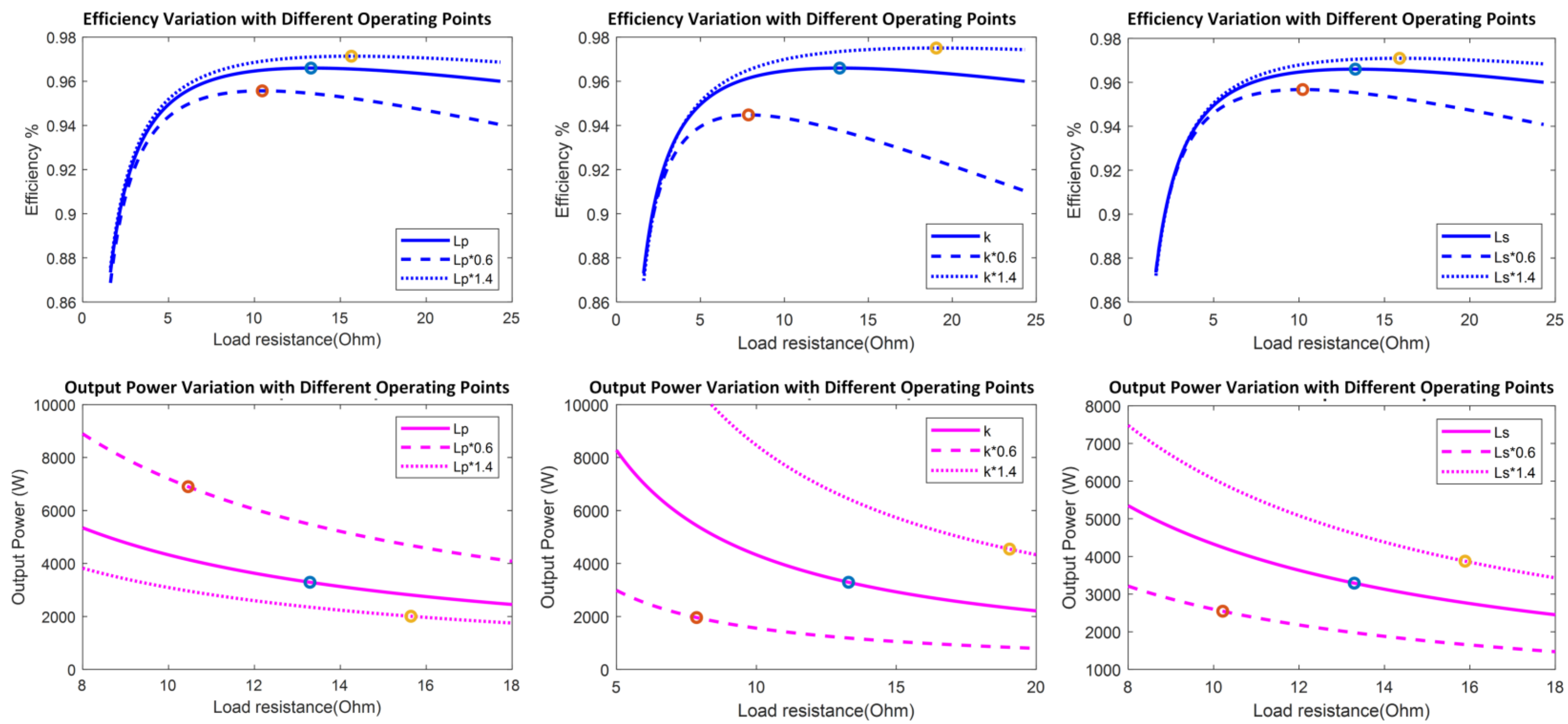

Figure 4-4 Efficiency and output power with different operating points while (a) Lp changes; (b) k value changes; (c) Ls changes.

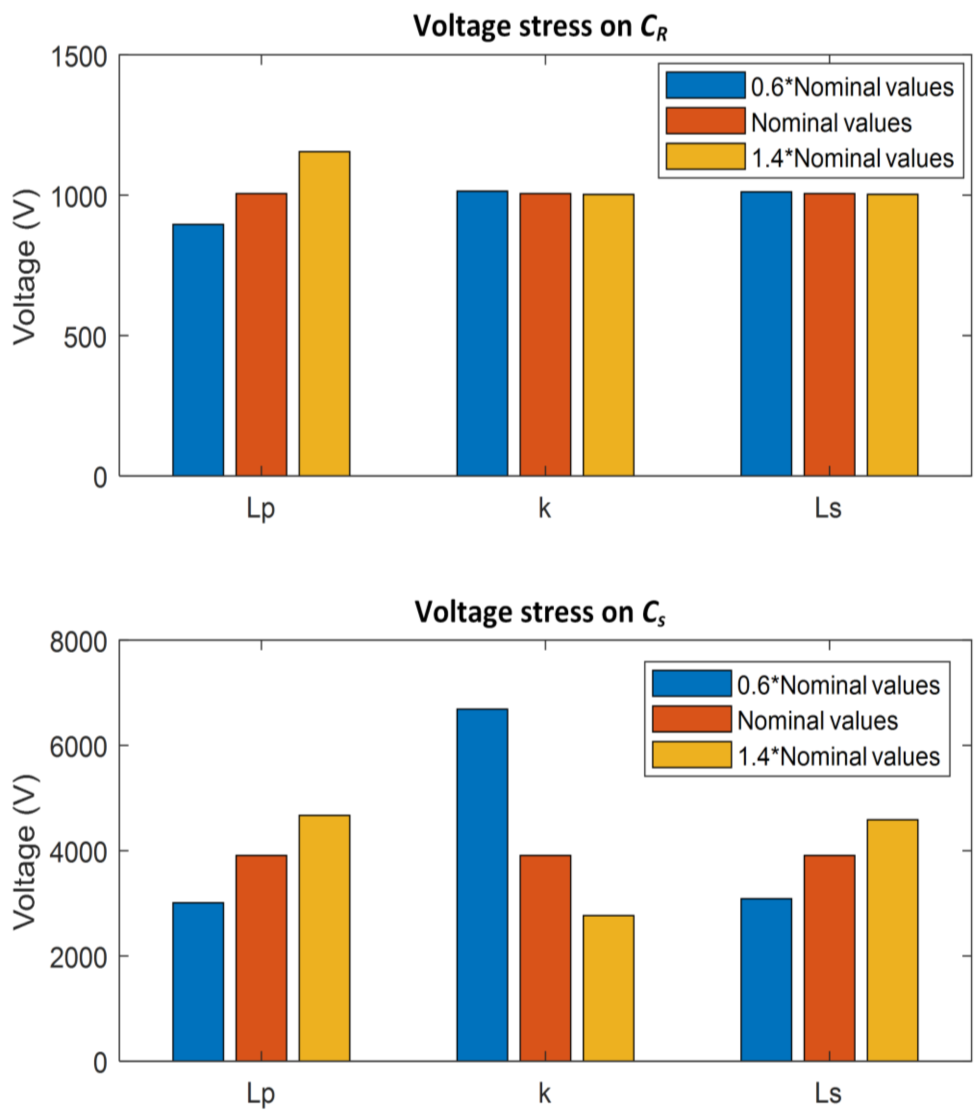

Figure 4-5 Voltage stress on compensated capacitors.

efficiency points in the top figures and the corresponding output power in the bottom figures. Besides, the voltage stress on C_R and C_s are also compared while the system operates at 5kW by varying L_p, L_s, and k. The detailed analysis results are shown in Figure 4-5.

The L_p variation effect on the system efficiency and the output power is shown in Figure 4-4 (a). By reducing the value of L_p, the power transfer capability is improved at the same R_{ac} value due to the increase of track current. The transferable power at the maximum efficiency is also lifted. However, more conduction loss on the transmitter leads to the reduction of the maximum efficiency. In addition, lower L_p shifts the maximum efficiency point to be closer to the efficiency drop cliff where in the low R_{ac} range, which will constrain the design to achieve a high output power with high efficiency. But lower L_p could reduce the voltage stress on both C_R and C_s, which increases the capacitor design flexibility as shown in Figure 4-5. The airgap impact on the efficiency and the output power is illustrated in Figure 4-4 (b). The k value change reflects the airgap variation between the transmitter and receiver. With a smaller airgap, the IPT system can elevate the power transfer capability as well as its efficiency. Besides, a smaller airgap also alleviates the voltage stress on C_s based on Figure 4-5. However, the airgap has limited flexibility in the railway application because the minimum gap distance is required between the bottom of the locomotive and the top of the tracks. Thus, the airgap should be designed as small as possible to ensure a higher transferable power and higher efficiency. Figure 4-4 (c) depicts the L_s variation effect on the output power and efficiency. Owing to the output voltage that is proportional to L_s and irrelevant to R_{ac}, the increase of L_s can improve the system efficiency and enhance the power transfer capability at the same time. But the trade-off is the compensation capacitor C_s requires a lower capacitance and carries higher voltage stress. In Figure 4-5, 40% increase of L_s leads to the voltage stress on C_s increasing from 3.9kV to 4.6kV with a capacitance reduction from 20.0nF to 14.3nF. This increases the capacitor design and selection difficulty, which becomes a drawback in improving the power transfer capability and system efficiency by increasing L_s.

Table 4-1 IPT system designed parameters.

Parameter	Symbol	Value
Tx self-inductance	L_p	70 uH
Rx self-inductance	L_s	175 uH
Coupling coefficient	k	0.236
Tx resonant inductor	L_R	70 uH
Tx capacitor	C_R	50.1 nF
Rx capacitor	Cs	20.0 nF
Operating frequency	f_0	85 kHz

The designed parameters are tabulated in Table 4-1 based on the analysis above. The parameter selection considered not only the parameter optimization but also the possible combination of the capacitors to meet the requirements of rated voltage and capacitance values, which ensures the design feasibility of the IPT system for railway applications.

4.4 Simulation Results

The 5kW IPT modular design was simulated via PLECS to validate the design. The designed parameters have been shown in Table 4-1. The IPT system aims to charge an 800V battery. Thus, a boost converter is connected to the IPT system to boost the voltage level. Since the LCL-S topology can provide a constant track current and constant output

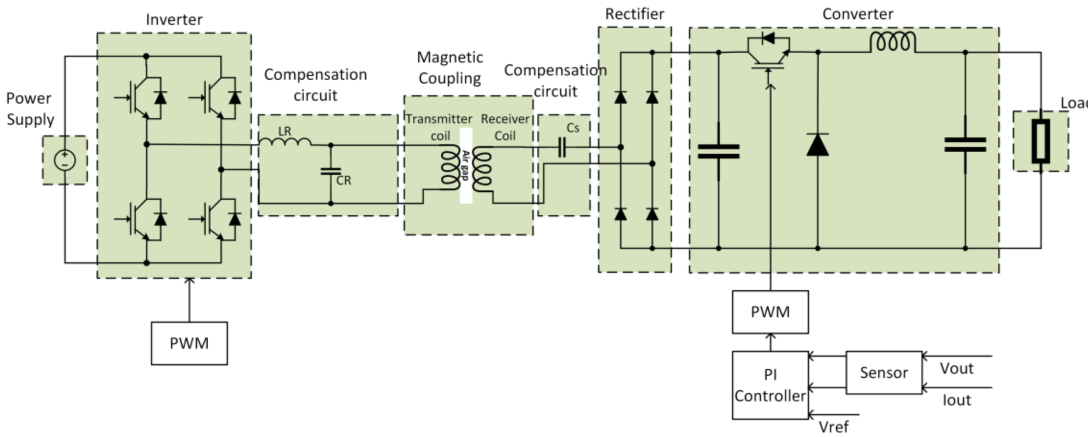

Figure 4-6 Circuit diagram of the designed IPT system.

voltage, the controller of the boost converter doesn't need communication with the IPT system. Figure 4-6 displays the circuit diagram of the designed IPT system for the railway application.

The system operates at 85kHz with an input DC voltage of 650V. The output voltage is 800V with an output power of 5kW. In order to validate its performance. The misalignment occurs at 1.5s by varying the coupling coefficient from 0.22 to 0.18 to observe the system response. Figure 4-7 demonstrates the simulation results of the track current as well as the output power. According to Figure 4-7 (a), the track current keeps a constant value of 14.6 A when the misalignment occurs. The system could still provide a 5kW output power when the misalignment occurs in Figure 4-7 (b). The rectifier output voltage is decreased because the coupling coefficient decreases in Figure 4-7 (c). Thus the voltage stress on the receiver side capacitor will be increased. The rated voltage and current of the receiver side capacitor should be carefully selected to allow the misalignment tolerance during the charging.

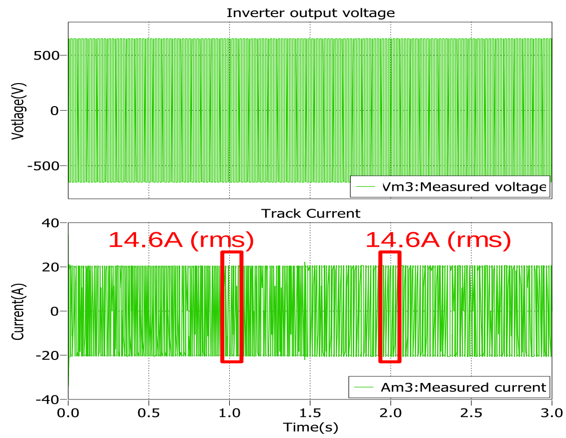

(a)

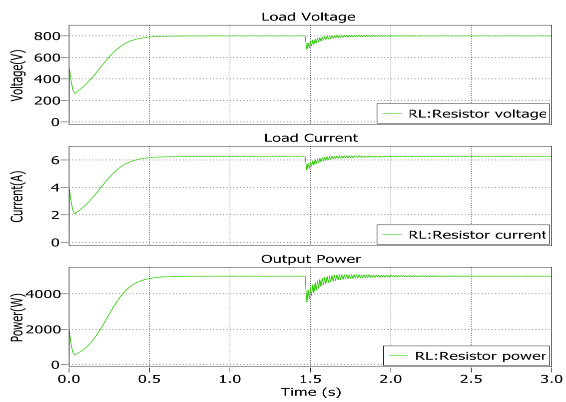

(b)

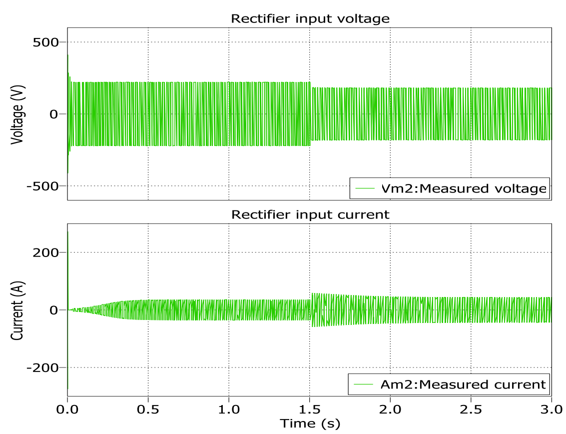

(c)

Figure 4-7 Simulation results of the designed IPT system. (a) inverter out voltage and current; (b) output information; (c) rectifier input voltage and current.

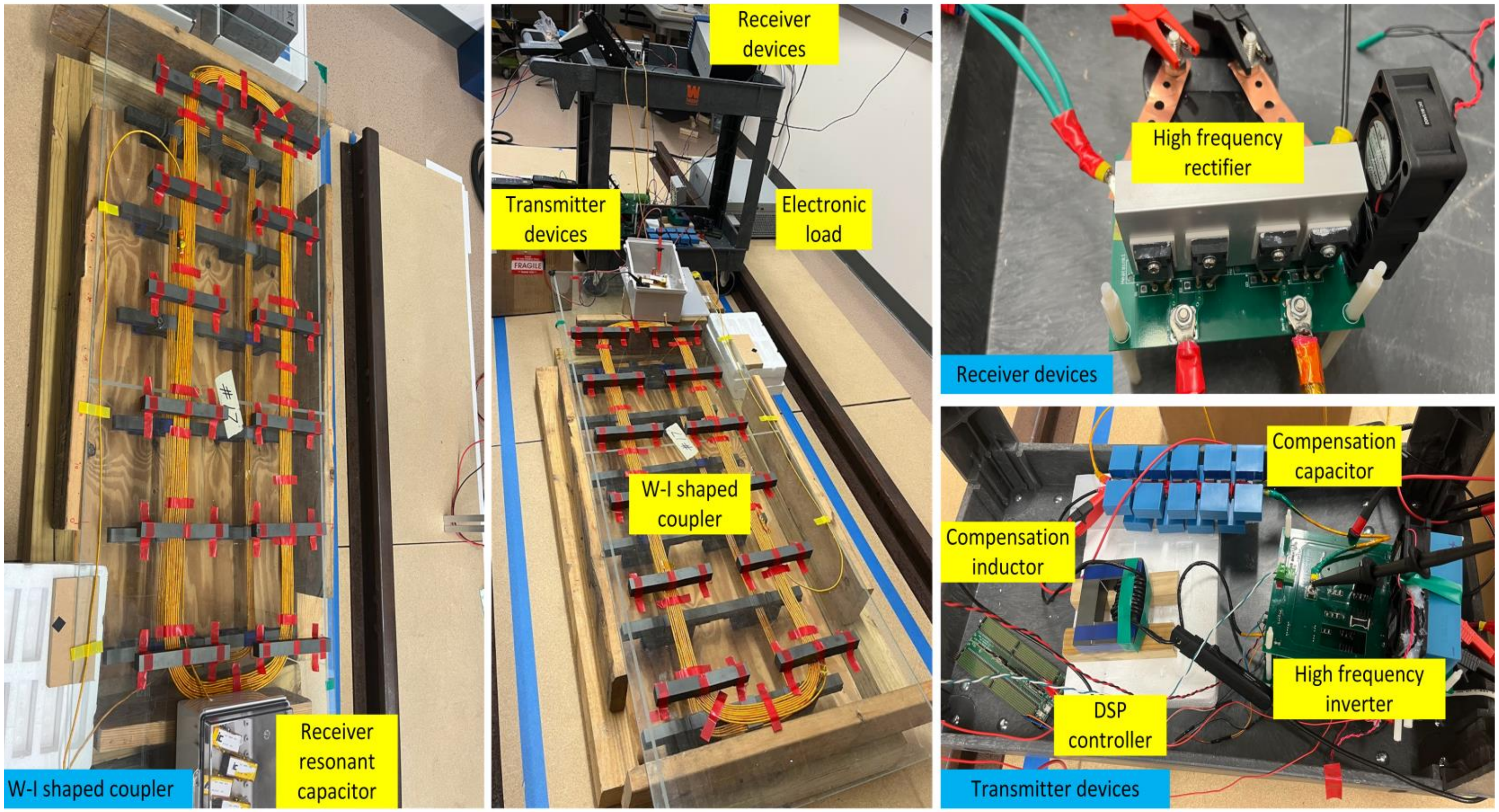

Figure 4-8 Prototype of the designed IPT system.

4.5 Prototype Development

In order to validate the performance of the W-I coupler and the LCL-S compensated IPT system design, a prototype was designed and implemented in the lab as shown in Figure 4-8. The prototype was designed to operate at 85kHz. A high-frequency (HF) inverter was developed with CREE C2M0080120D Silicon-Carbide MOSFET to provide the HF power to the coupler. The components in LCL-S circuit were connected by Litz wires to alleviate skin-effect and reduce the conduction loss in the coils. Since the transmitter and receiver coils are also required to carry high voltage stress, the Litz wires are wrapped by Kapton tapes to provide the high voltage insulation. The HF rectifier is composed of four C5D50065D Schottky diodes. The material of W-I cores is 3C90 from Ferroxcube. The transmitter compensation capacitor bank is composed of eighteen B32656S2224 film capacitors to attain 48.4nF with a 7.2kV rated voltage. The receiver compensation capacitor bank is five HC1 high power resonant capacitors in series to obtain 20nF with 5kV rated voltage. The measured parameters of the IPT prototype are tabulated in Table 4-2. The measured coupling coefficient is 0.215 at 5 inches airgap, which matches the FEA and simulation results.

4.5.1 Power and Efficiency Testing

The IPT prototype with the proposed W-I coupler was tested by ramping up the input voltage from 150V to the rated 650V with 8.5Ω load resistance. The simulation results and testing results are shown in Figure 4-9. The simulation model is built in PLECS by taking not only the conduction losses but also the switching losses of the semiconductor devices into consideration to improve the simulating precision. The DC-DC efficiency was measured by Tektronix PA3000 Power Analyzer. The testing output

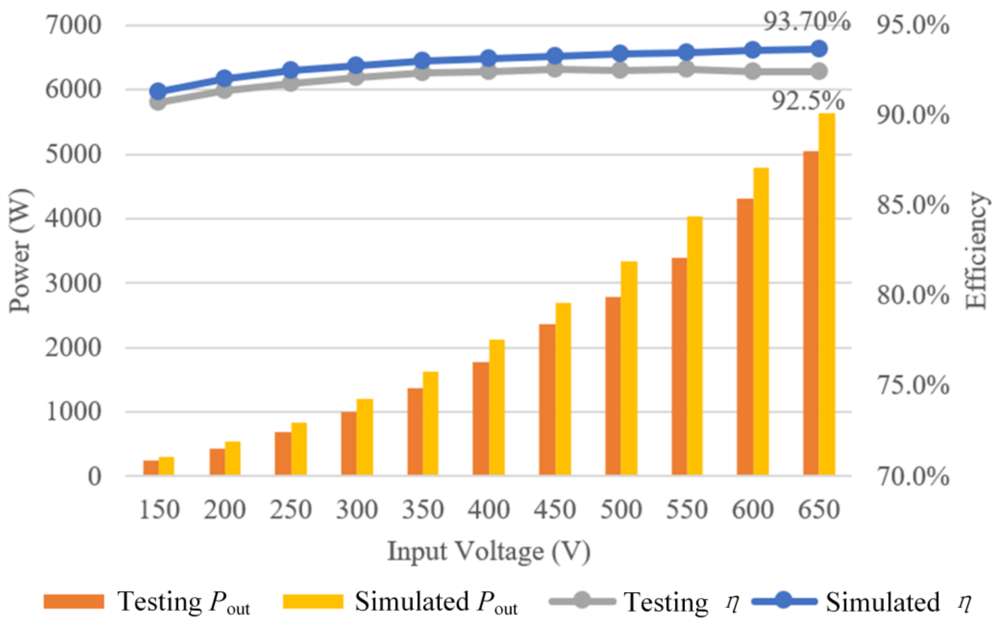

Figure 4-9 Experimental results of the output power and efficiency variation.

Table 4-2 Measured parameters of the IPT prototype.

Parameter	Measured Value
L_p	70.4 μH
L_s	174.6 μH
L_R	70.5 μH
C_R	48.4 nF
C_s	20 nF
C_{dc}	120 μF
k	0.215
f	85 kHz
R_{dc}	8.5 Ohm
Airgap	5 inch

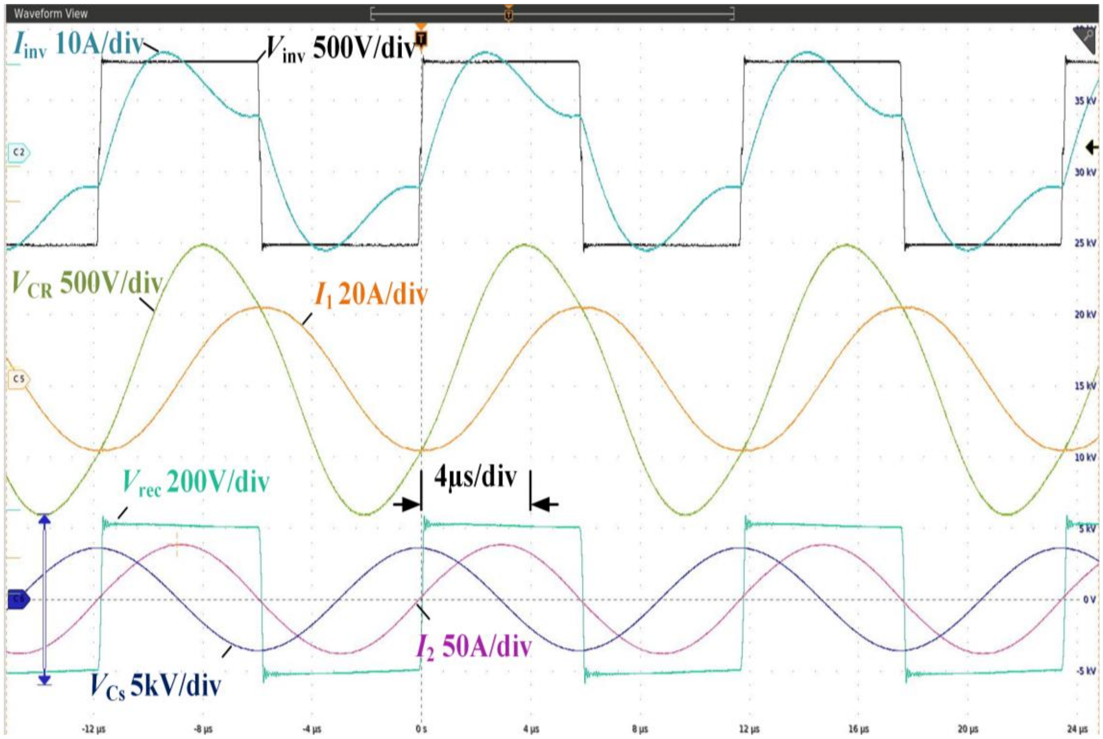

Figure 4-10 Experimental waveforms of the IPT system.

power was lifted from 265W to the rated power 5kW with a system efficiency from 90.7% to 92.5%. The output power and the efficiency of the simulation results were slightly higher than the testing results because of the tolerance from passive components values, ESRs, and the coupler installation. Figure 4-10 illustrates the working conditions at 5kW rated power. The inverter output voltage is a square wave with a peak value of 650V. Since the compensation circuit operates near the resonant point, the coil and capacitor voltage values are much higher than the input and output voltage values. Figure 4-10 shows the Rx side capacitor voltage, also equals to the Rx coil voltage, is 3.6kV. Because of the characteristics of the LCL-S compensation circuit, the inverter is operated at ZVS condition, which will reduce the switching losses and improve the system efficiency. The track current is a constant value of 15A, which is irrelevant to the *k* value and load variation.

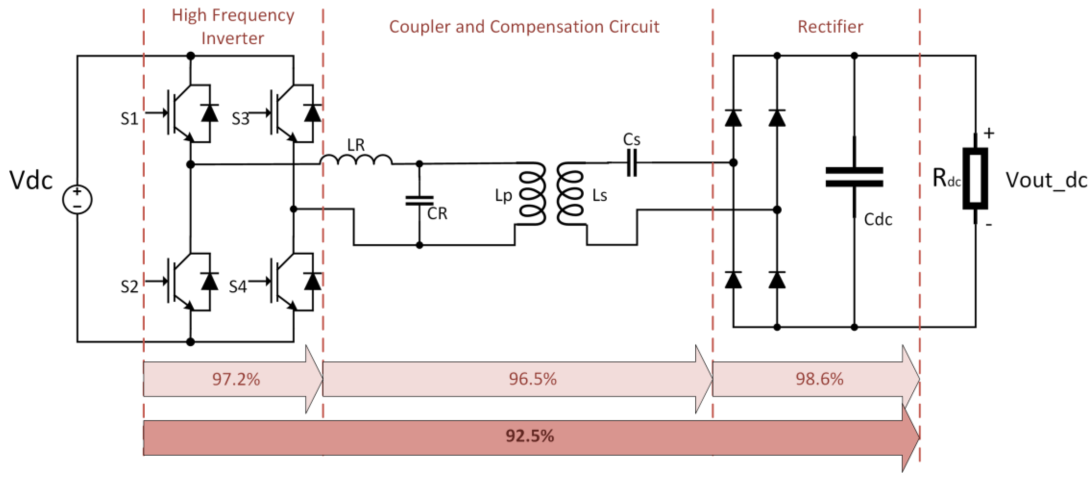

Figure 4-11 System efficiency measurement results for the IPT prototype.

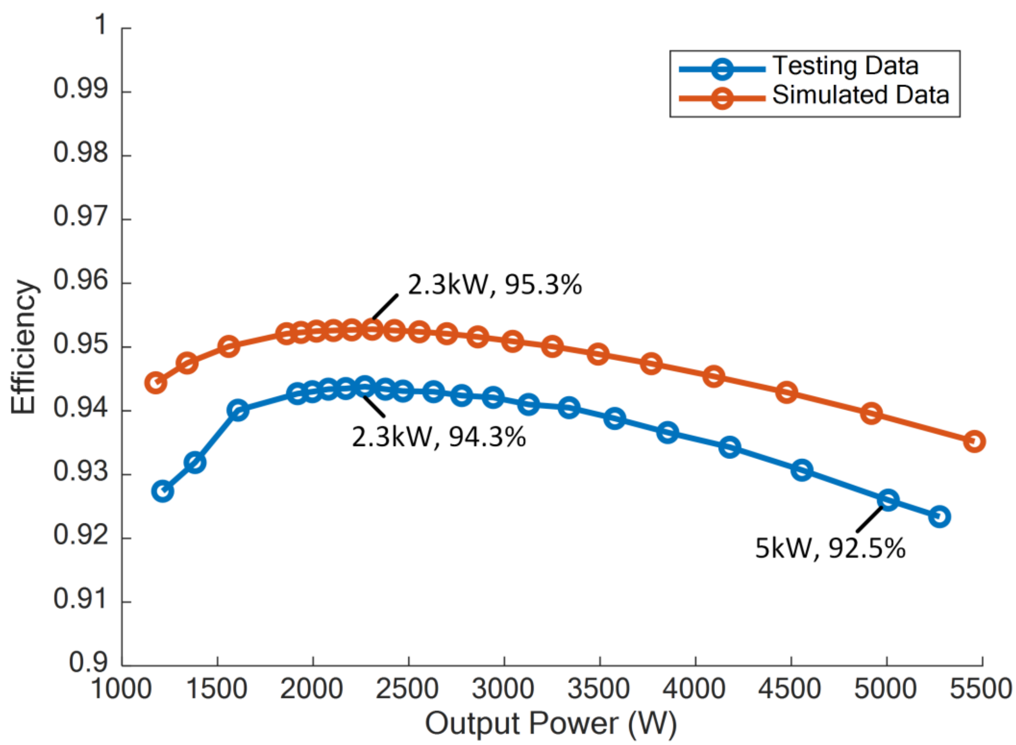

Figure 4-12 Testing results of different operating points at rated input voltage.

The output power of the W-I coupler based IPT prototype at 650V input voltage is 5kW with a DC-DC efficiency of 92.5%. This is the highest IPT system efficiency reported for railway application to the best of the author's knowledge. The efficiency in the high-frequency section is also estimated by an oscilloscope and is demonstrated in Figure 4-11. The efficiencies for DC/AC inverter, coupler and compensation circuit, and rectifier stages are 97.2%, 96.5%, and 98.6%, respectively. The experimental results validate the feasibility of the W-I shaped LCL-S compensated IPT system design.

The prototype was also tested at the rated input voltage of 650V with Rdc variation. The output power and efficiency testing results are shown in Figure 4-12. The proposed W-I shaped IPT system can reach to the highest DC-DC efficiency of 94.3% while the system is operating at 2.3kW, which matches the simulation results. Besides, the designed operating point could be different from the maximum efficiency point to achieve a higher output power, as long as the voltage stress on the passive components does not exceed the maximum voltage. According to the testing results, the system could improve the output from 2.3kW to 5kW by only sacrificing 1.8% efficiency.

4.5.2 Misalignment Testing

To validate the misalignment performance of the W-I coupler, the system was tested in different misalignment positions from 0cm to 50cm with an increment of 10cm as shown in Figure 4-13. The self-inductance of the transmitter and receiver, as well as the k value variation, were measured and shown in Figure 4-14. Since the misalignment changes the magnetic circuit whereby changing the receiver position, the transmitter and receiver self-inductance was reduced by 0.64% and 2.34%, respectively. The coupling coefficient was reduced by 37%, which will impact the power transfer capability as well

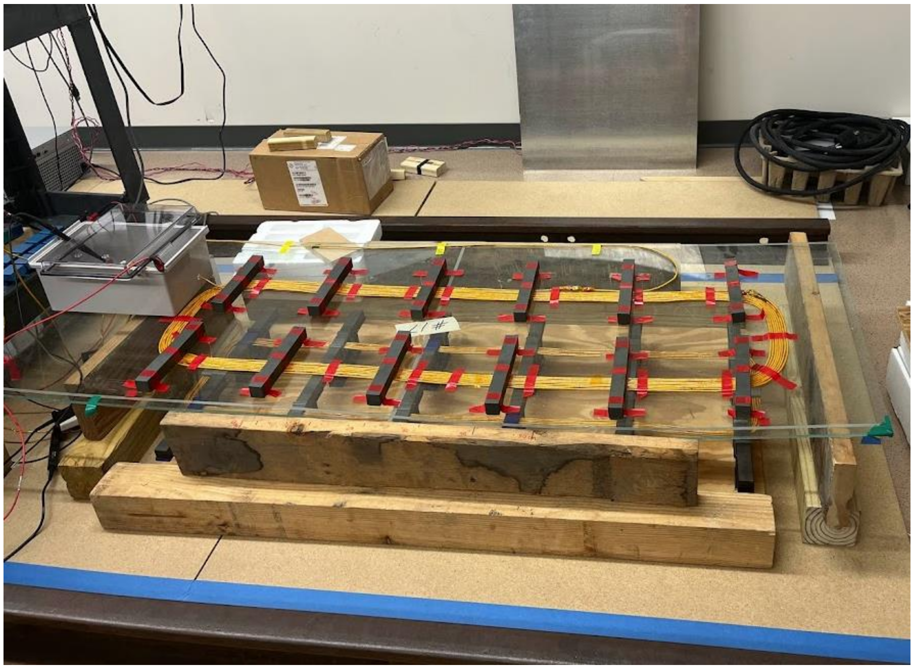

(a)

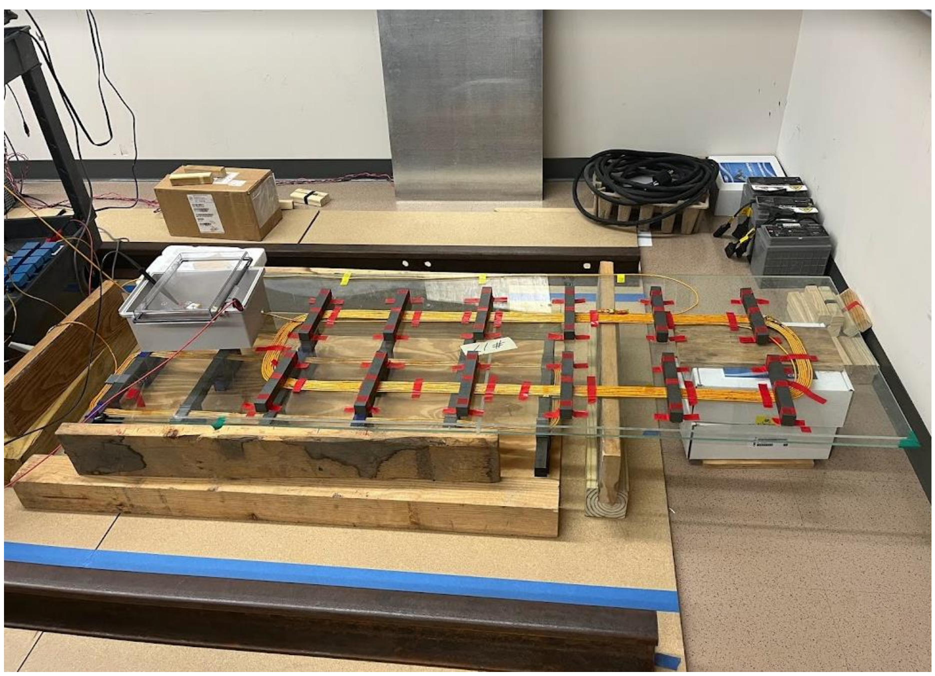

(b)

Figure 4-13 Experimental setup of the IPT prototype with (a) 0 cm misalignment; (b) 50 cm misalignment

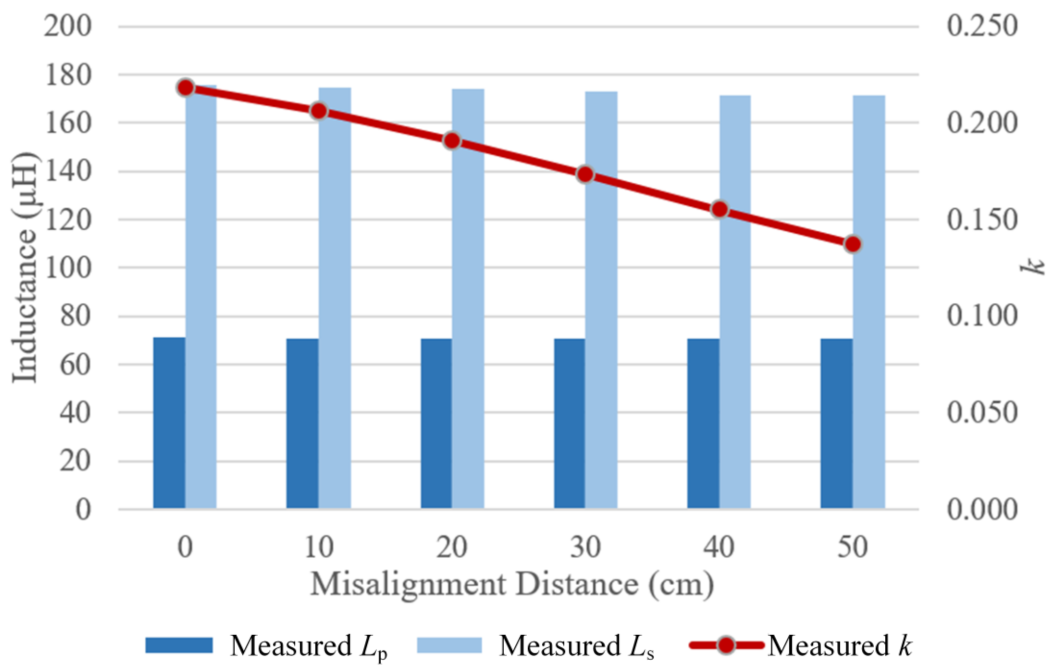

Figure 4-14 Misalignment impact on k and self inductance.

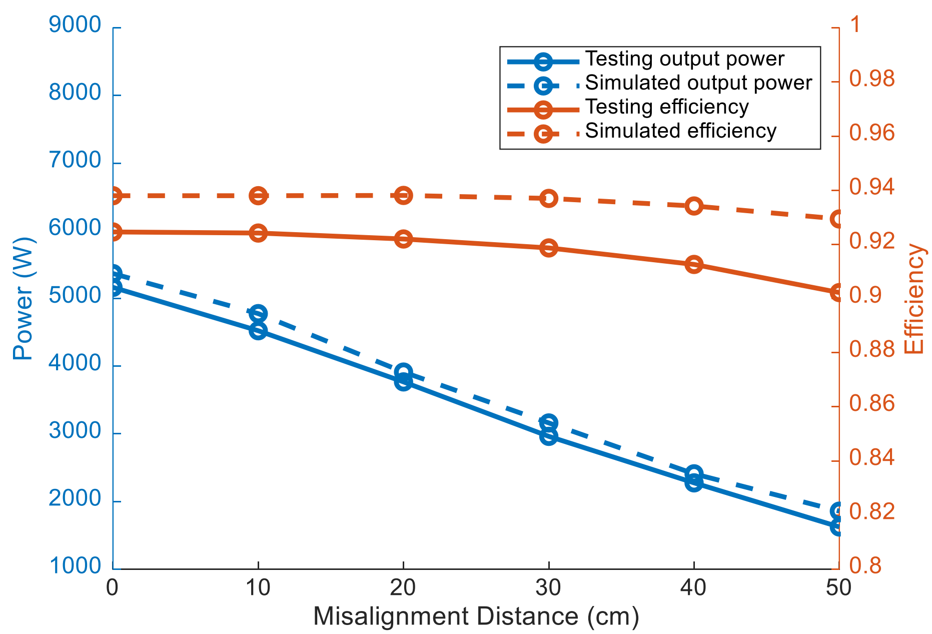

Figure 4-15 Misalignment impact on the output power and efficiency.

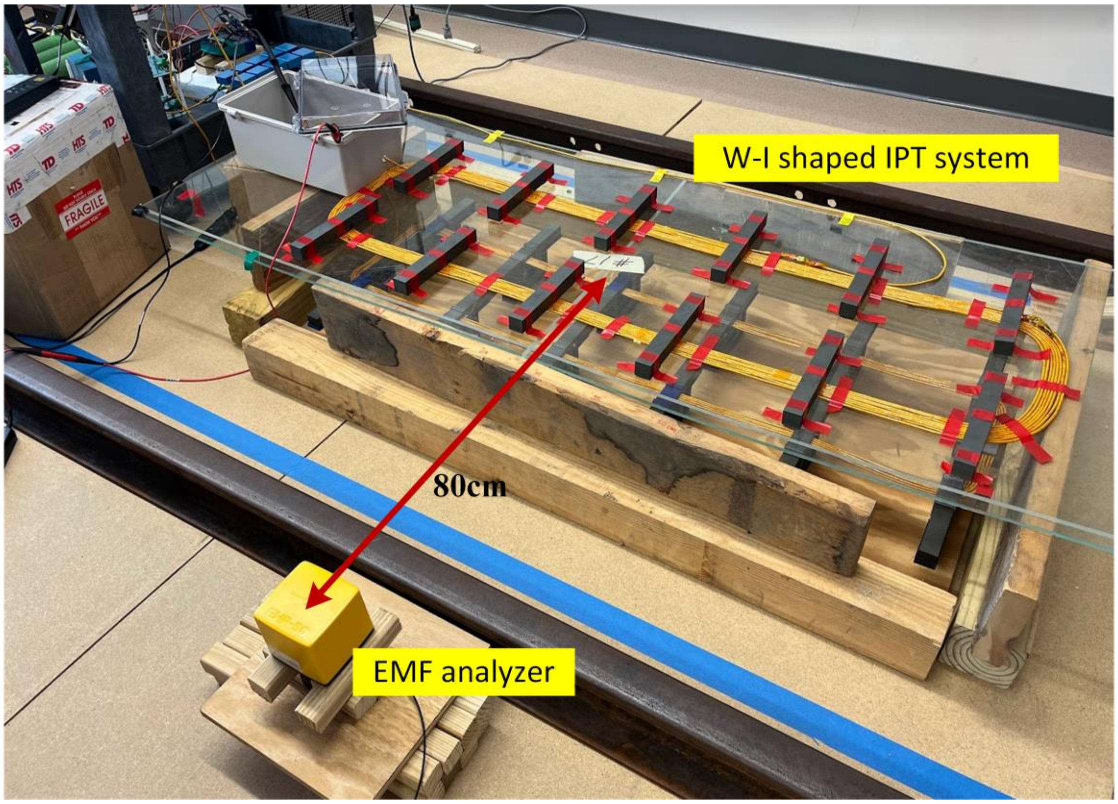

Figure 4-16 Experimental setup of the EMF measurement.

as the system efficiency. Figure 4-15 depicts the misalignment impact on the output power and efficiency. By giving the 650V input voltage and 8.5Ω load resistance, the output power was dropped from 5kW to 1.8kW, whereas the efficiency could still maintain at more than 90%. The measured output power has a good match with the simulation results. The efficiency difference between the simulation and experiment comes from the inductor value design and the ESRs measurement tolerance.

4.5.3 Electromagnetic Field Testing

In order to assess the electromagnetic field (EMF) emission surrounding the proposed IPT system, The EMF testing experiment was conducted and shown in Figure 4-16 using EHP-50F field strength analyzer. The testing point was setup 80 cm away from the center of the coupler. This point is also about the edge of a locomotive, which is the closest point that humans might be exposed to the EMF. International Commission on Non-Ionizing Radiation Protection (ICNIRP) 2010 drew up the guidelines of EMF exposure at frequencies <100kHz, which was used to evaluate the EMF emission for the design IPT system. The guideline noted that EMF exposure should be no more than 27μT for human safety purposes [63]. By implementing the EMF measurement experiment, the measured EMF at the testing point is 12.4μT at 85kHz with a 5kW operating condition, which meets the ICNIRP 2010 standard.

CHAPTER 5: FREQUENCY MODULATED MPPT METHOD FOR IPT SYSTEMS

5.1 Motivation

Electric vehicles are gradually being used for residential and industrial transportation since they have no tailpipe emissions which harms the environment, and they are much quieter than conventional vehicles. The general method to charge an EV is conductive charging. However, this method always has bulky power cords to be manipulated, as well as the potential of electric shock hazards during the charging procedure. To overcome these concerns, wireless charging technology has been developed rapidly in recent years that brings convenience and a safer way to charge EVs. Inductive power transfer is the most common method to charge the EVs wirelessly, because of the unique requirements of EV charging that include power rating, airgap distance, system efficiency, and electromagnetic interference concerns, etc. A typical IPT system consists of a transmitter system and a receiver system. The concept uses the electromagnetic coupling between the transmitter and the receiver to transfer the power wirelessly. For loosely coupled IPT systems, the compensation circuits are also required on both transmitter and receiver sides to maximize the power transfer capability and improve the system efficiency. Many research teams have investigated and developed high-power EV wireless charging systems with high performance, some of which have been commercialized and introduced in Chapter 2. However, most of the wireless charging system designs did not consider the coupler inductance's factory-producing tolerance. An investigation has been conducted on the fixed inductor tolerance and the wireless charging coil inductor tolerance in the market [74]. According to the datasheet investigation shown

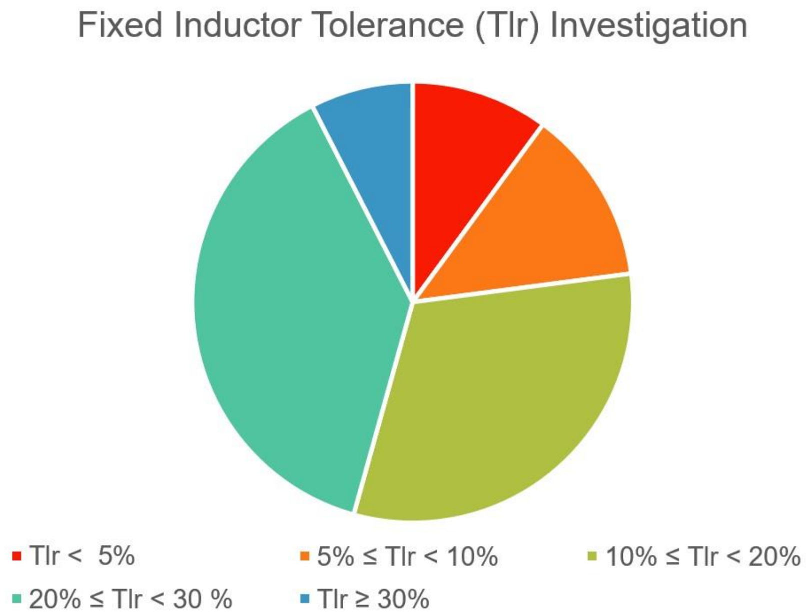

(a)

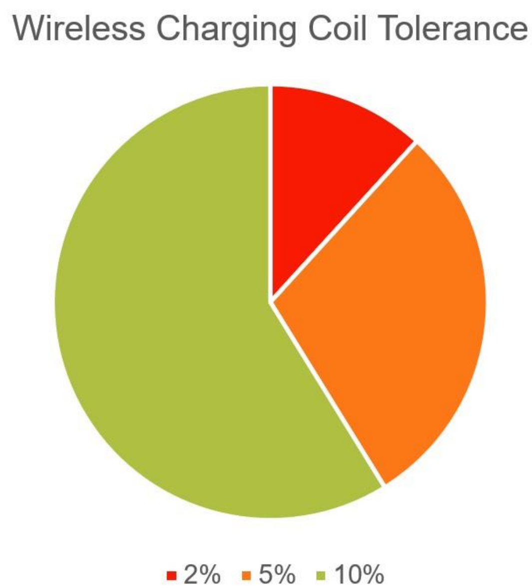

(b)

Figure 5-1 Inductance tolerance investigation. (a) Fixed inductor tolerance; (b) Wireless charging coil inductance tolerance.

in Figure 5-1 (a), 83% of fixed inductor manufacturing tolerances in the market are more than ±10%. Figure 5-1 (b) displays the coil inductor tolerance for the wireless charging application. More than half of the manufacturing tolerance for wireless charging coil is also ±10%. Thus, the general tolerance of an inductor from factories is around ±10%. The coupler inductance might also change while the ambient temperature and humidity vary. Besides, the misalignment of the coupler will also lead to the inductance variation in an IPT system. These variations will change the resonant point of the system which will weaken the power transfer capability significantly. Due to the change of coupler inductance, some of the IPT systems might not be able to work at their maximum power points. In order to tune the system to achieve the maximum power point, [70] proposed a tracking method by adjusting the frequency and capacitance value. [73] also proposed a method to optimize the values of passive components to mitigate the system sensitivity. But these methods are only applicable to the design stage. When the system is manufactured, the factory tolerance cannot be compensated to achieve the maximum power point. [71] created a capacitor matrix to track the impedance matching point. However, the capacitor matrix will increase the cost of the system by adding multiple switches and extra capacitors. [72] also presented a tuning method to track the optimized operating frequency, but the tuning time is too long as 3 seconds.

This chapter proposed a frequency modulated maximum power point tracking (MPPT) method to adjust the system to achieve its maximum power transfer capability within the system constraints. It could track the maximum power point by finding the optimized frequency to improve the power transfer capability weakened by the inductance variation. The impact of inductance tolerance on the system power transfer capability is analyzed based on an LCL-S compensated IPT system. The simulation results of the proposed MPPT method validate the feasibility under different inductance variation conditions.

5.2 Inductance Variation Impacts on IPT Systems

The equivalent circuit of the LCL-S IPT system has been shown in Figure 4-2. The design constraints of this compensation circuit are $\omega L_R = 1/\omega C_R$, $L_R = L_P$, and $\omega L_S = 1/\omega C_S$, where L_R is the transmitter resonant inductance, C_R is the transmitter resonant capacitance, L_p is the transmitter coil self-inductance, L_s is the receiver coil self-inductance, C_s is the receiver compensation capacitor, and ω is the angular frequency. This compensation topology can keep the track current I_1 constantly regardless of the coupling coefficient k and the equivalent load R_{ac} change, which is a common compensation circuit for wireless charging systems. The method in [54] was applied to simplify the circuit to derive the input impedance Z_{in}, which reflects the power transfer capability of IPT systems in a constant input voltage condition. The receiver side equivalent impedance Z_s is,

$$Z_s = j\omega L_s + \frac{1}{j\omega C_s} + R_{ac} \tag{5.1}$$

The reflect impedance Z_r from the receiver side to the transmitter side is derived as follows,

$$Z_r = \frac{-j\omega M I_2}{I_1} = \frac{\omega^2 M^2}{Z_s} \tag{5.2}$$

where M is the mutual inductance between transmitter and receiver coils, and I_2 is the induced current in the receiver coil. The input impedance Z_{in} could be derived as follows,

$$Z_{in} = j\omega L_R + \left(\frac{1}{j\omega C_R}\right) // \left(j\omega L_p + Z_r\right)$$

$$= j\omega L_R + \frac{\frac{L_p}{C_R} + \frac{Z_r}{j\omega C_R}}{\frac{1}{j\omega C_R} + j\omega L_p + Z_r} \tag{5.3}$$

Therefore, the system apparent power S is expressed as,

$$S = {V_{in}}^2 / Z_{in} = Re(S) + jIm(S) \tag{5.4}$$

In order to quantify the system, the designed parameters in Table 4-1 were used for the frequency sweep analysis to observe the power variation. Since the equivalent model does not take the losses into consideration, *Re(S)* which could be defined as output power *P* represents the power transfer capability of the IPT system. According to Equation 5.3 and 5.4, the output power can be modulated by varying operating frequency or the equivalent load Rac. In order to find the updated resonant point, the system was analyzed

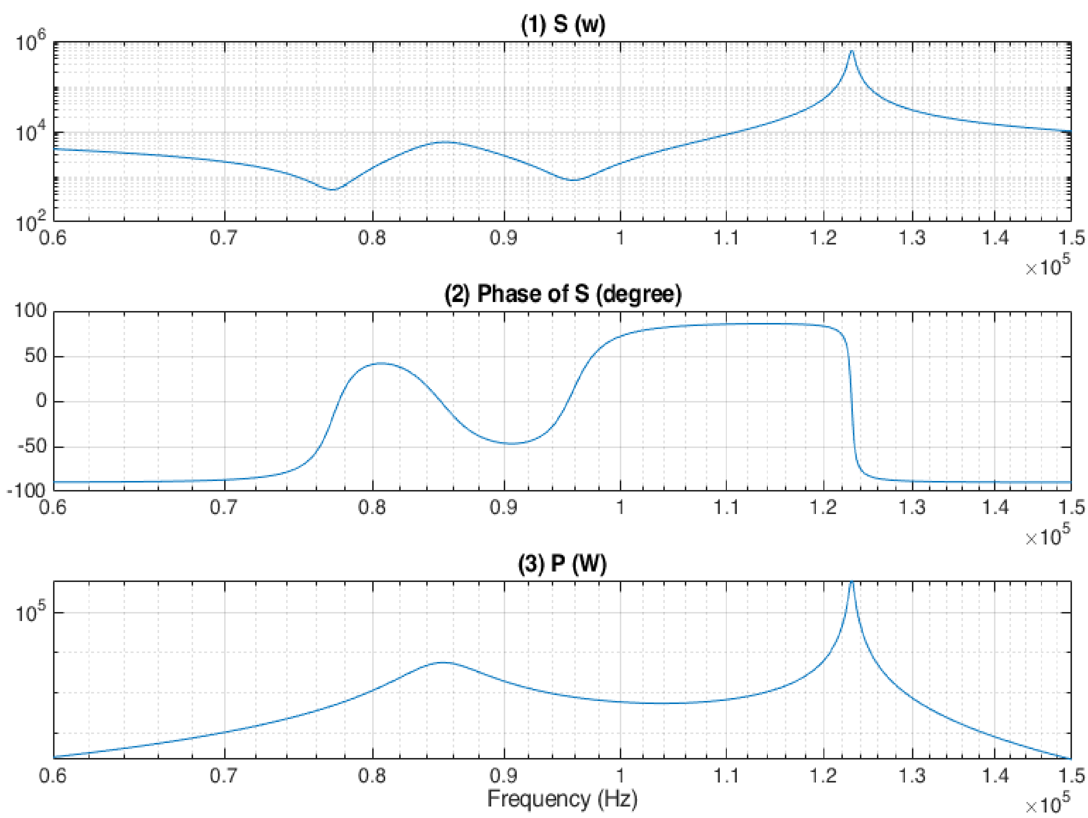

Figure 5-2 Frequency sweep of the IPT system.

under a constant resistance load condition. Figure 5-2 depicts the frequency sweep results based on the designed parameters. There are two peak values based on the results. One peak value is the working condition when the system is operating at its designed frequency of 85 kHz with a designed output power of 5.7 kW. Another peak value is shown at 123 kHz with much higher output power. Although this condition is the maximum point in the frequency sweep, this operating point is extremely unstable since the phase of *S* varies sharply around this point, as well as the power rating has far exceeded the design requirements. Thus, the working condition at 85 kHz is considered to be the reasonable maximum power point.

When the system has the inductor coils with a manufacturing tolerance, the power transfer capability will reduce with fixed frequency control. Figure 5-3, Figure 5-4, and Figure 5-5 demonstrate the L_R, L_p, and L_s variation impacts on the system power transfer capability, respectively. The x-axis has been normalized to be f / f_0, which f_0 = 85 kHz. In Figure 5-3, the output power reduces from 5.7 kW to 5.6 kW at 85 kHz while the LR varies ±10%. The maximum power point reduces by 0.1% while L_R increases 10%, and by 0.7% while L_R decreases 10%. Therefore, the variation of L_R impact on power transfer capability can be negligible. In Figure 5-4, the change of L_p does not lead to the maximum power point drifting, however, the power transfer capability increases from 5.7 kW to 6.3 kW when there is an inductance change of +10%, and decreases to 5.1 kW when the inductance change is -10%. In the meanwhile, inductance variation makes *Im(S)* not zero at the maximum power condition, which will cause a higher VA rating and lead to higher conduction losses. In Figure 5-5, the change of L_s reduces the output power by 61.3% (from 5.7 kW to 2.2 kW) while L_s has a variation of ±10%, which limits the power transfer capa-

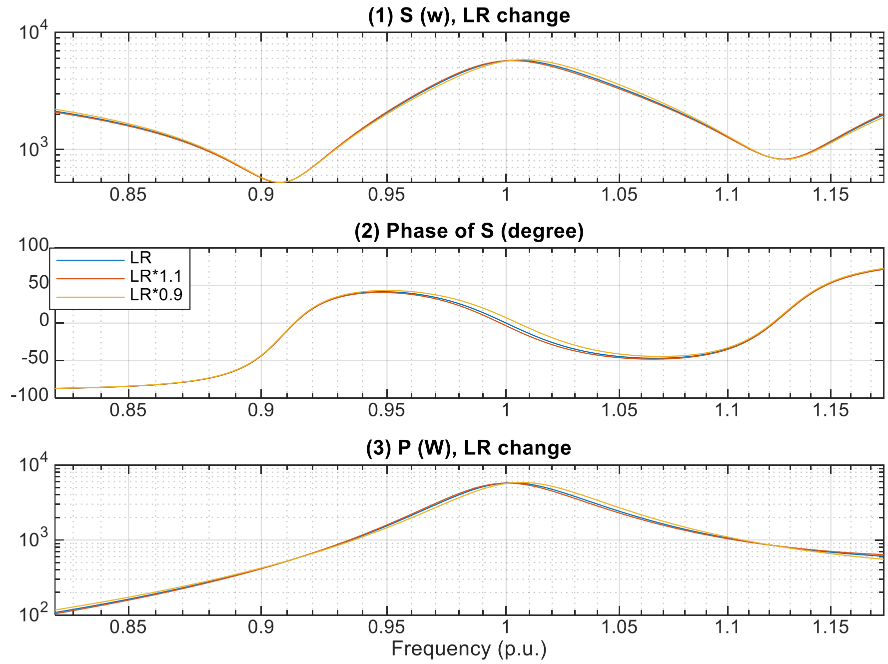

Figure 5-3 L_R variation effects.

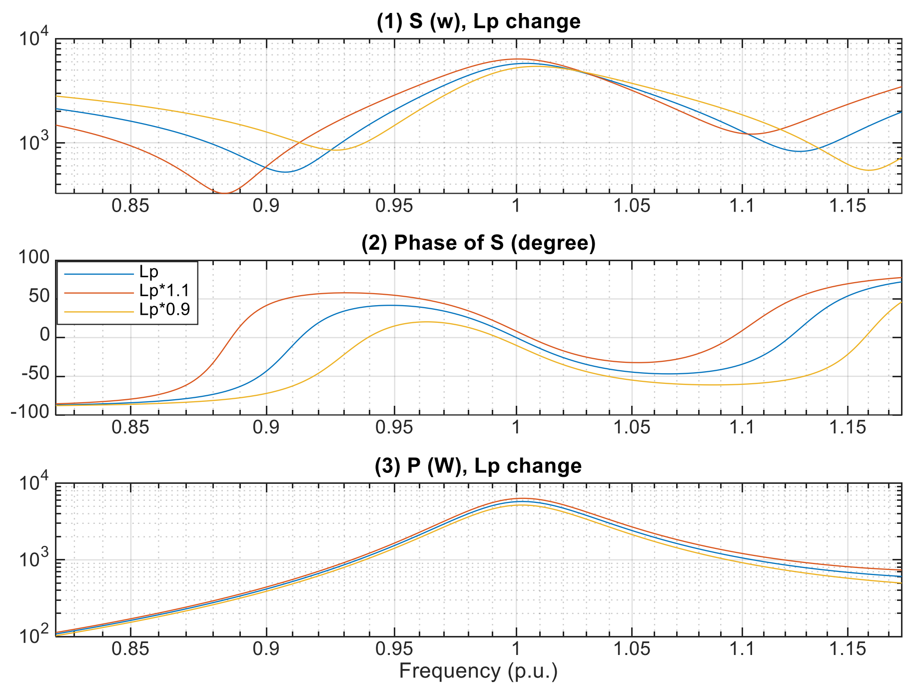

Figure 5-4 L_p variation effects.

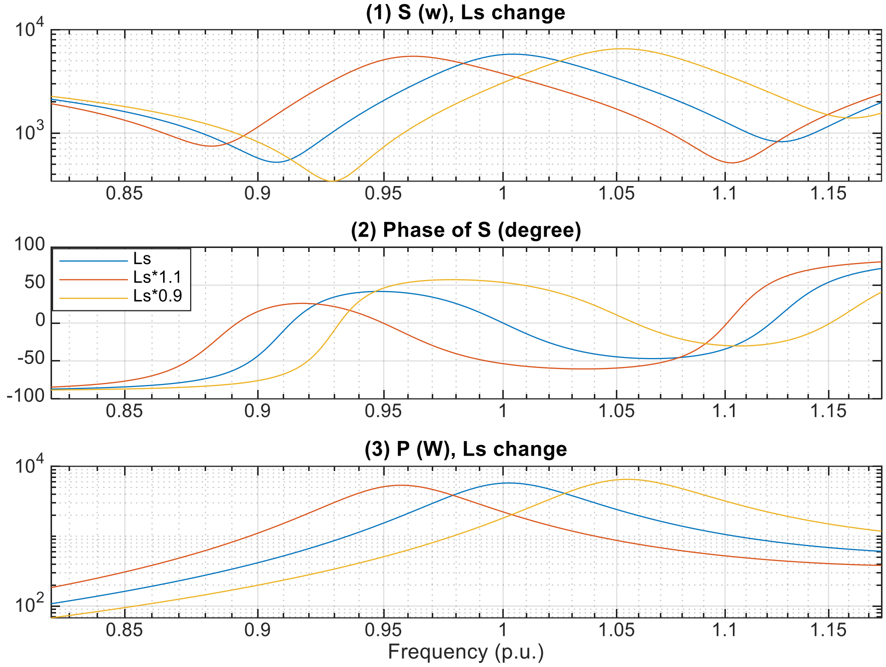

Figure 5-5 L_s variation effects.

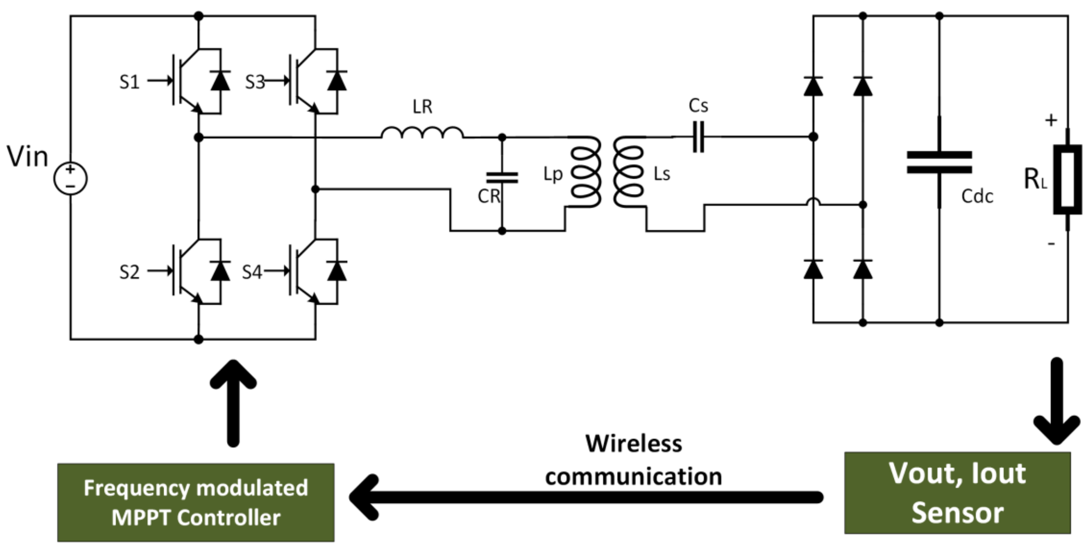

Figure 5-6 LCL-S compensation IPT system diagram with the frequency modulated MPPT controller.

bility significantly. The operating frequencies to achieve the maximum power point are shifted by ±5% when L_s changes ±10%.

Thus, the inductance variation, especially the L_s change, has a great impact on the power transfer capability of the IPT system. The frequency needs to be constrained in a reasonable range to maintain the maximum power transfer capability and meet the design requirements during the frequency controller design.

5.3 Proposed Frequency Modulated MPPT Method

A frequency modulated MPPT method was proposed to optimize the system to its maximum power transfer point by adjusting the operating frequency. This method can not only be applied for the design stage to find the optimized operating frequency, but also can adjust the frequency for the application stage to maximize the power transfer capability against the inductance variation caused by factory manufacturing tolerance and environment change. In a typical LCL-S compensated IPT system depicted in Figure 5-6, the measured output power will be fed to the MPPT controller of the inverter, in order to track the power and optimize the frequency to achieve the maximum power point. The flow chart of the frequency modulated MPPT is shown in Figure 5-7. The frequency increment Δf needs to be appropriately selected, to reach the maximum power point faster and to ensure the stability of the IPT system. The frequency modulation boundary is also required to ensure the voltage and current in each component will not exceed the designed rating. The frequency boundary also provides the benefits to meet the frequency range requirement from the WPT standard for real-world applications. Besides, it can maintain the stability of the controller and the system. This frequency range is determined by the co-

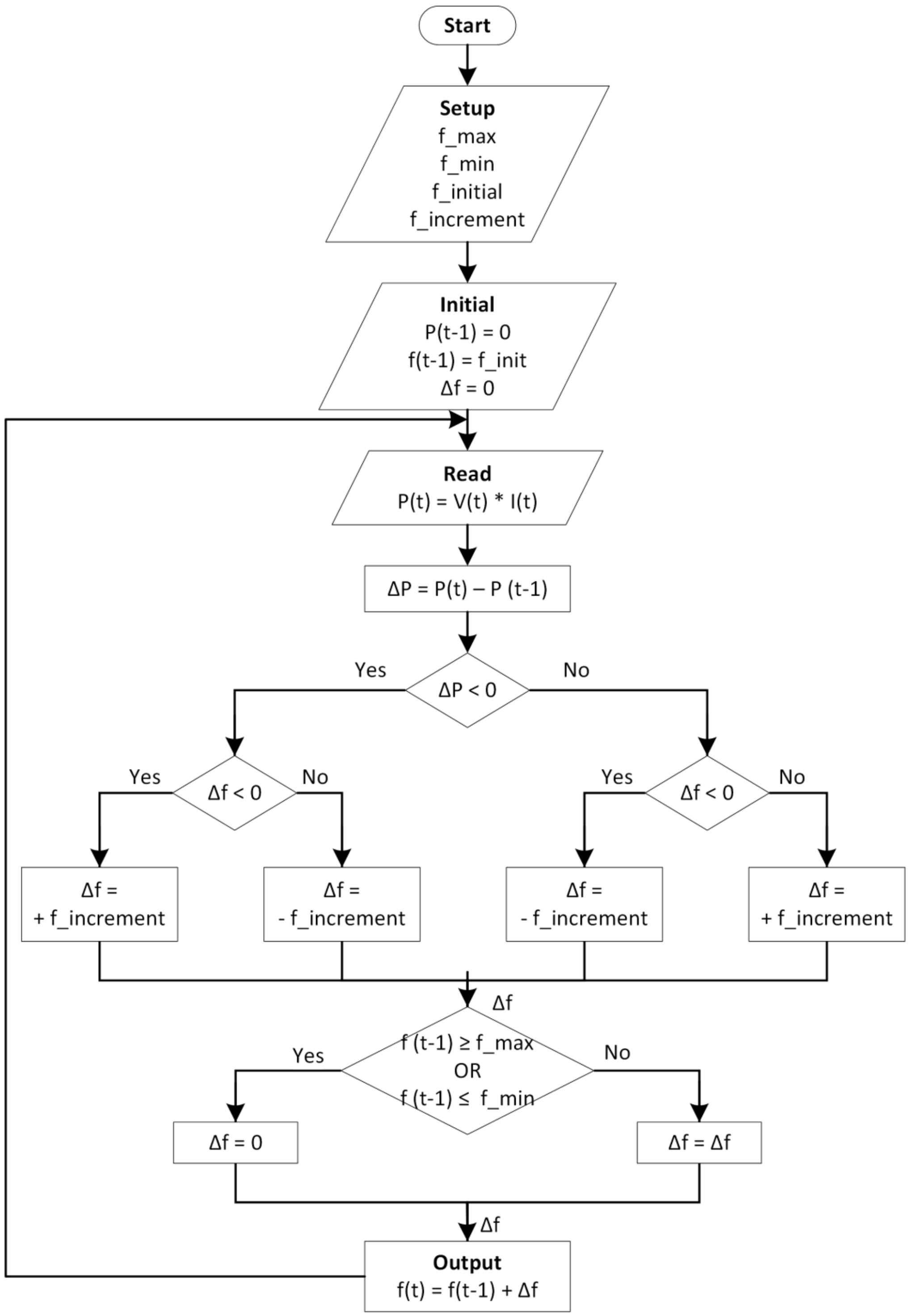

Figure 5-7 Frequency modulated MPPT algorithm

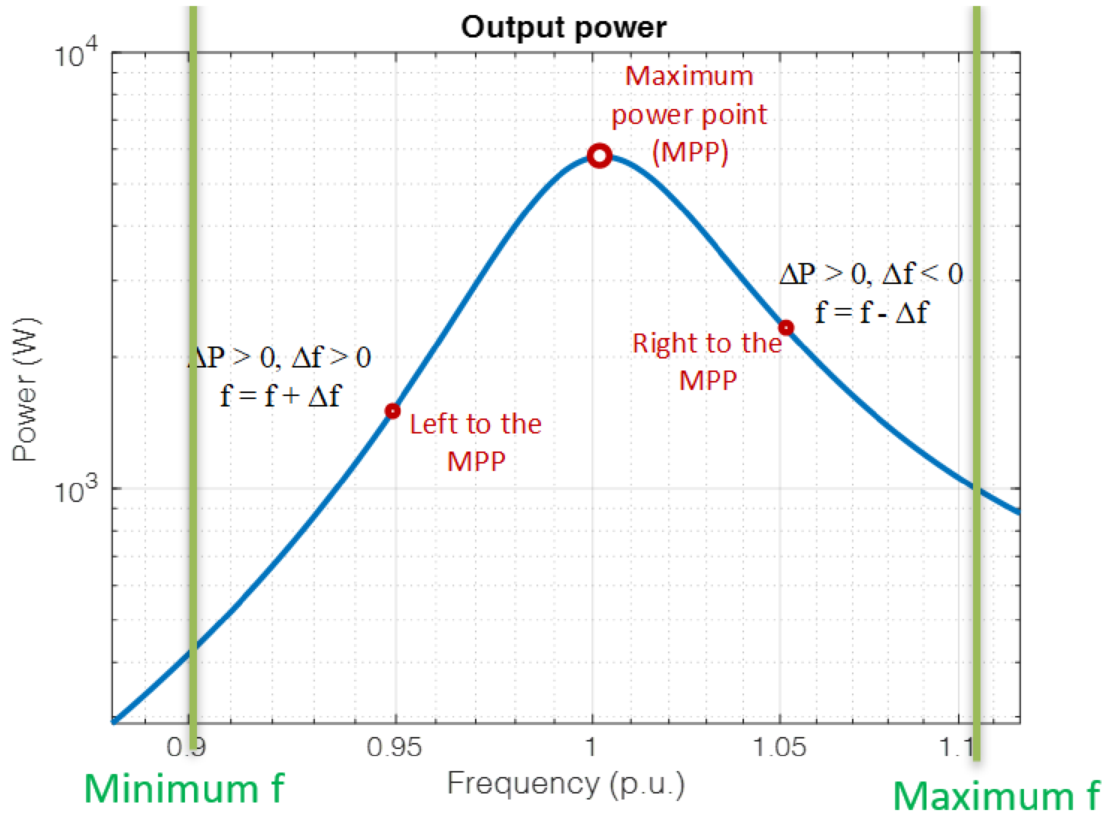

Figure 5-8 Frequency modulated MPPT method.

mpensation topology as well as the design parameters. Noted that this frequency modulated MPPT method was investigated under a constant resistance load to find its optimal operating frequency. Before enabling the MPPT controller, the maximum and minimum frequency, initial frequency, frequency increment, and the sampling time are required to be setup in the controller. Then, the controller compares the output power change and decides to increase or decrease the frequency. A visualization figure of the frequency based MPPT controller is shown in Figure 5-8. The operating points are on the left side of the MPP, the operating frequency is gradually increased, while the operating points are on the right side of the MPP, the frequency is gradually reduced to improve the output power. Due to the frequency range constraint, the frequency will not exceed the boundary through the system has not reached to its MPP.

The feasibility of the frequency modulated MPPT method was validated via the simulation. Since the Ls variation changes the maximum power point drifting most, the simulation varied the value of Ls to change by ±10% to observe if the proposed frequency based MPPT method could optimize the frequency and track the maximum power point. The increment frequency was 100 Hz with a sampling time of 0.5ms to ensure a fast response time. The frequency range was designed from 78 kHz to 92 kHz.

Figure 5-9 demonstrates the simulation results of the modulating procedure. The IPT system is designed to be 5 kW rated power at 85 kHz. The nominal designed parameters are shown in Table I. The frequency modulated MPPT is enabled at ten milliseconds (ms). While the L_s decreases by 10% as shown in Figure 5-9 (a), the output power is weakened to be only 1.6 kW because of the manufacturing tolerance. After enabling the frequency modulated MPPT controller, the frequency is gradually increased with an increment of 100 Hz. The final optimized frequency is around 89.7 kHz, with a transient time of 26 ms. The output power is increased by 3.6 times, from 1.6 kW to 5.8 kW. While the L_s increases by 10% as shown in Figure 5-9 (b), the output power is 2 kW before enabling the frequency modulated MPPT controller. The frequency starts to decrease after enabling the frequency modulated MPPT controller. The output power is optimized to 4.8 kW after the modulation, which increases by 2.4 times. The final optimized frequency is around 81.5 kHz, with a transient time of 17 ms.

In order to validate the frequency boundary setup, the inductor tolerance of L_s is set to be ±20% for validating the corner case of the controller. Figure 5-10 displays the simulation results of the modulating procedure. When the inductance of L_s has a tolerance of -20%, the frequency could be modulated to around 95 kHz when the controller has no

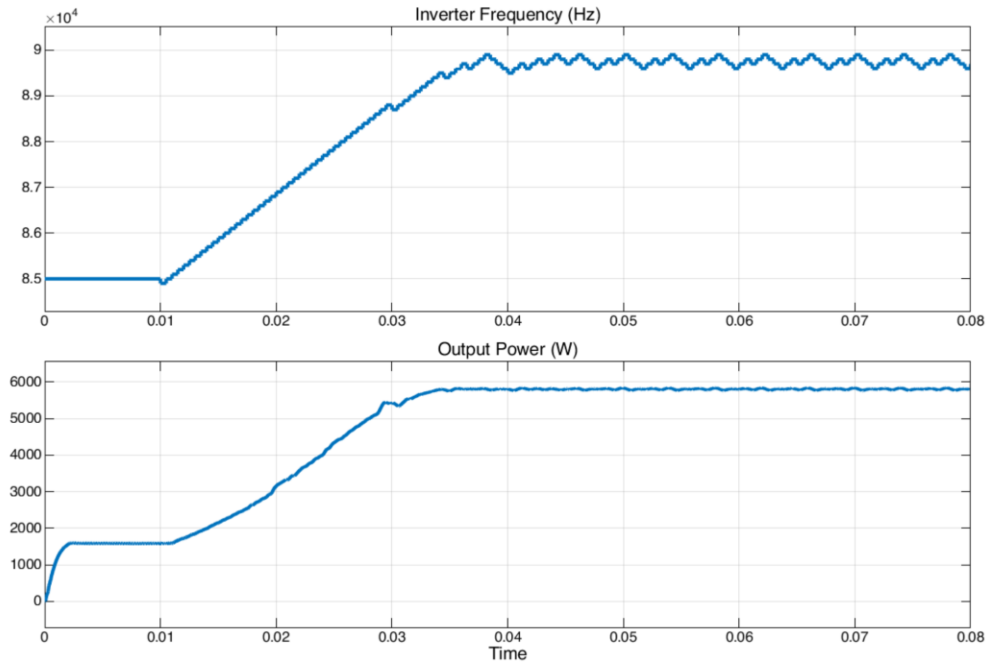

(a)

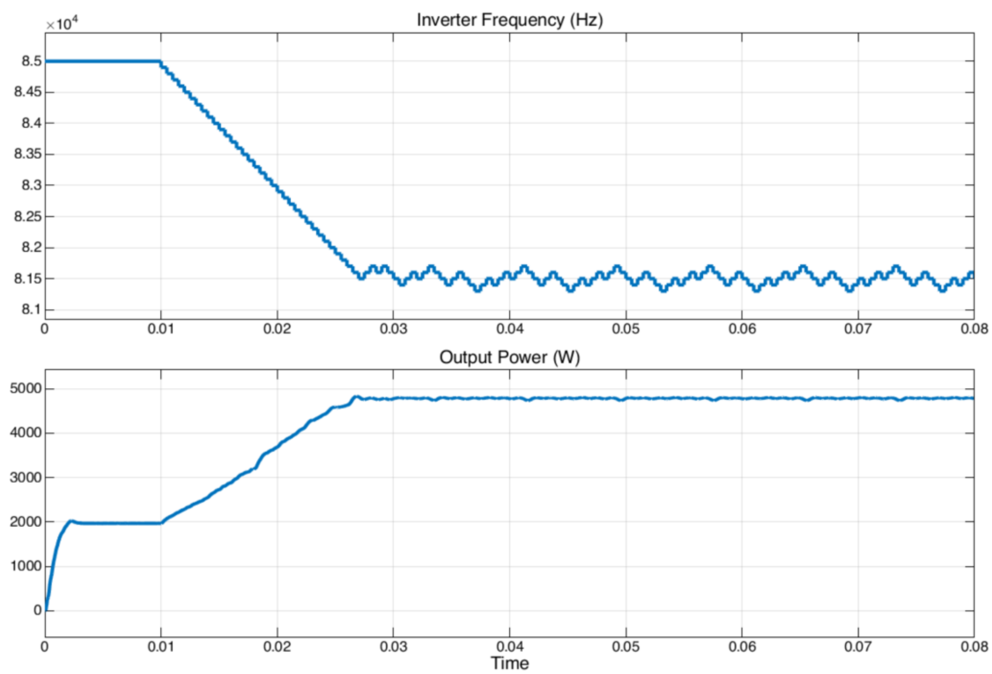

(b)

Figure 5-9 Simulation results of the frequency modulated MPPT controller. (a) Lp decreases by 10%; (b) Lp increases by 10%.

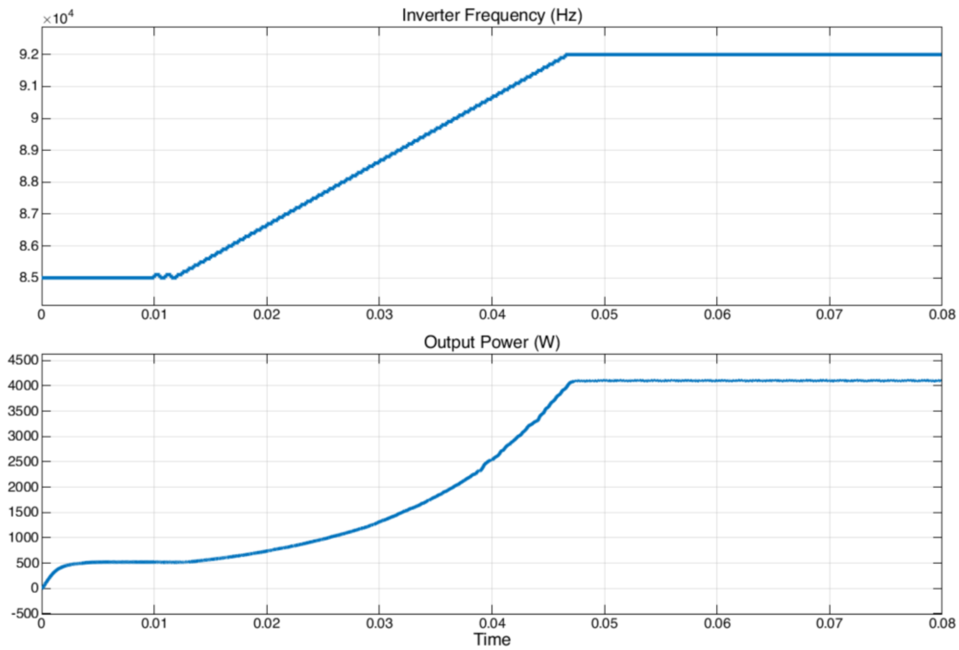

(a)

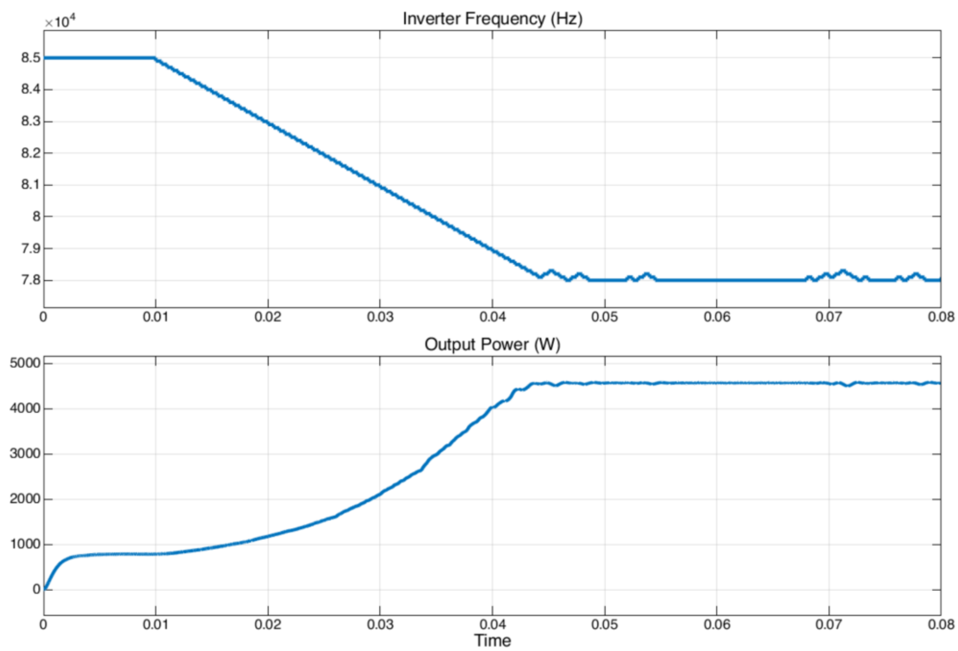

(b)

Figure 5-10 Simulation results of the frequency modulated MPPT controller. (a) Lp decreases by 20%; (b) Lp increases by 20%.

boundary setup. However, the higher operating frequency will increase the voltage and current stress in the IPT system exceeding the designed rating and potentially damaging the system. Therefore, the boundary to limit the frequency range is required. Figure 5-10(a) demonstrates that the system is operating at its maximum frequency boundary when the inductor has a tolerance of -20%. The power transfer capability is improved by 8.2 times from 0.5 kW to 4.1 kW. Figure 5-10(b) shows the system is operating at its minimum frequency boundary when the inductor has a tolerance of +20%. The power lifts from 0.8 kW to 4.6 kW, while the frequency is clamped at its minimum edge of 78 kHz.

5.4 Experimental Results

To validate the frequency based MPPT method, an LCL-S compensated IPT system shown in Figure 4-8 has been implemented for testing. The detailed design procedure has been described in Chapter 3 and 4. According to the analysis of inductance variation for the LCL-S IPT system, the change of L_s weaken the output power most compared with other inductor parameters. Thus, the receiver coil was changed from 175 μH to 195 μH to mimic the factory inductance tolerance. The initial operating frequency is designed to be 85kHz with a constant load of 8.5Ω. The frequency modulated MPPT controller was setup a frequency range from 78kHz to 92 kHz, with an increment of 100 Hz. Sampling time was settled to be 0.5 ms for the controller. The voltage and current were collected from a voltage and current sensor and imported to the Digitial Signal Processing (DSP) TI28379 for processing.

It was tested at an input voltage of 250V with an 8.5 Ohm resistance to observe the power transfer capability variation. The first experiment is to perform a frequency sweep to the IPT system with an inductance tolerance, in order to observe the updated maximum

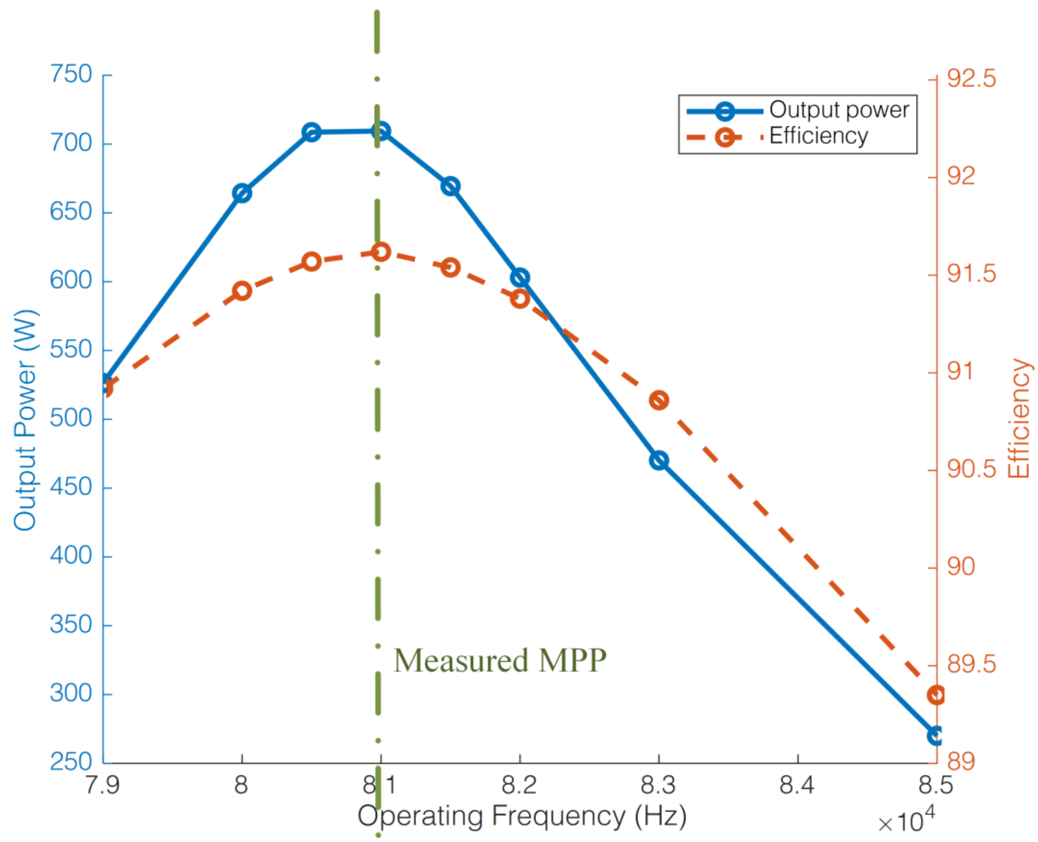

Figure 5-11 Maximum power point and efficiency testing.

output power point and the updated operating frequency. The experimental results are depicted in Figure 5-11. The frequency sweep was conducted from 79kHz to 85kHz, while the output power and the DC-DC efficiency were measured and demonstrated. The maximum power point is 710 W when the operating frequency is 81 kHz. The updated MPP is also the maximum efficiency point with an efficiency of 91.6%, because of the operating resonant point with a minimum VA rating. The IPT system only has an output power of 270W with an initial operating frequency of 85kHz. The power transfer capability can improve by 2.6 times if the frequency is optimized to compensate the inductor tolerance.

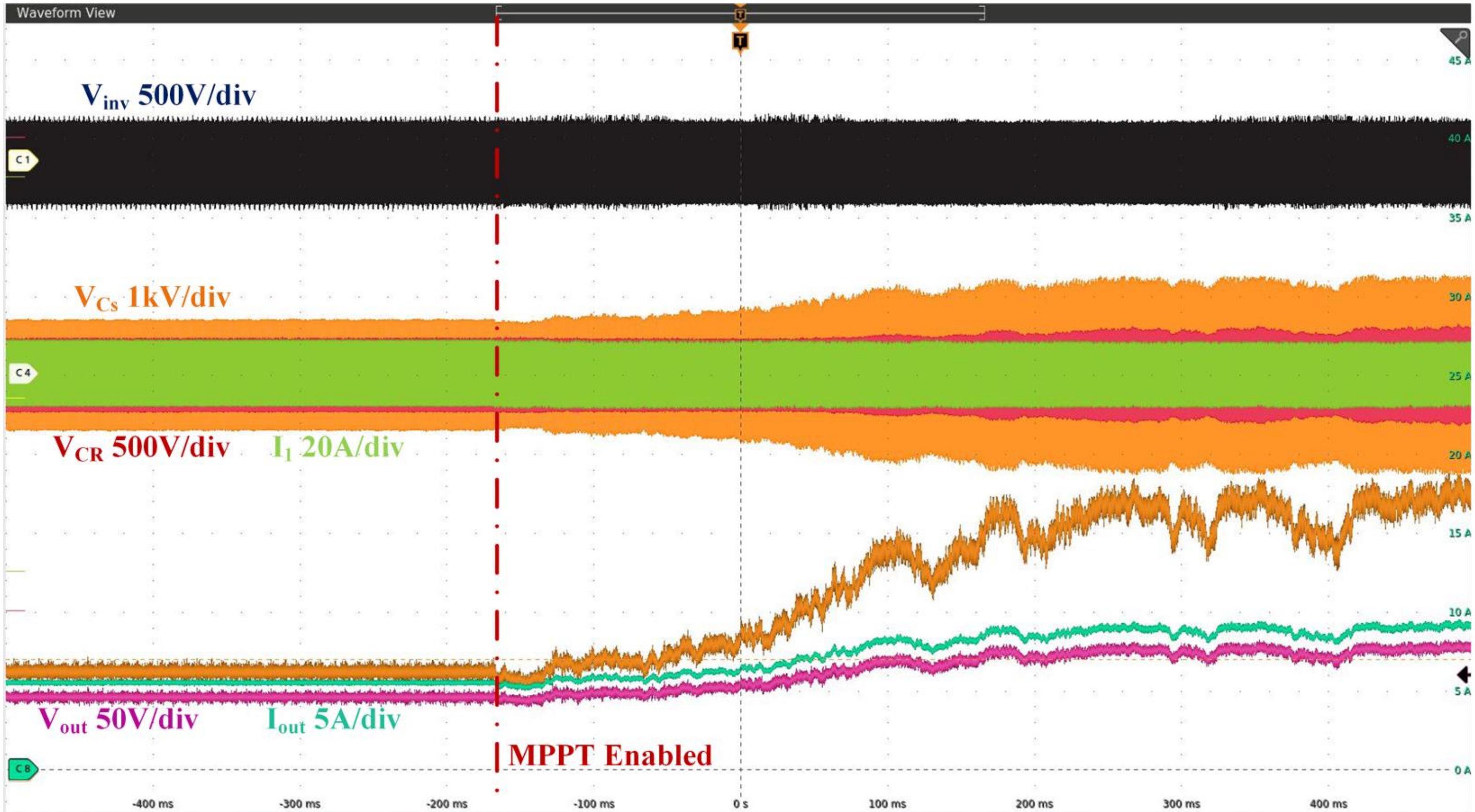

Figure 5-12 Testing results of the frequency modulated MPPT controller.

The efficiency can also be optimized from 89.4% to 91.6% if the frequency can be modulated.

Then the frequency modulated MPPT method was tested in the same working condition described above to validate the functionality. The modulating results are shown in Figure 5-12. When the MPPT was enabled, the output power was improved from 230W to 710W. The operating frequency is also modulated from 85 kHz to around 81kHz, which matches the MPP testing in the frequency sweep. The track current can still maintain at 5.7A without the effect of the frequency change. The voltage stresses at C_R and C_s are increased because of the improvement of the output power. The transient time to find the optimized frequency point is 320 ms. The longer transient time is caused by the signal noise on the DSP input side. When the system operates at the optimized operating point, the output power also has a power drop issue due to the noise. The future work will optimize the voltage and current sensor hardware to minimize the noise and reduce the power fluctuations.

CHAPTER 6: CONCLUSION AND FUTURE WORKS

6.1 Conclusion and Contributions

The motivation and the huge potential of the wireless power transfer technology for railway applications were investigated. The technical gap in achieving wireless charging for the railway was also discussed in detail.

A W-I shaped coupler is proposed to wirelessly charge the rail locomotives based on the current challenges and gaps of IPT technology for the railway application. The optimization and analysis of the W-I shaped coupler were conducted in terms of geometry and size. The W-I shaped coupler has a relatively higher coupling coefficient and a significantly lower core volume, which can reduce the core material cost and maintain the power transfer capability. Its modular design is easy to extend to achieve a higher power rating and is compatible with static and dynamic charging.

An LCL-S compensated IPT system was designed and optimized to achieve system stability during misalignment and load variation due to the constant track current irrelevant with load and misalignment change. The design eliminates the communication between transmitter and receiver to simplify the control algorism design. The optimized LCL-S circuit simplifies the components for higher system efficiency. The parameter was also optimized and designed to achieve a higher system efficiency.

The prototype of the W-I shaped coupler based IPT system was implemented. The prototype was validated at 5 kW with 92.5% DC to DC efficiency, which is the highest IPT system efficiency reported for railway applications. The misalignment performance of the IPT prototype was tested, which matched the simulation results. The EMF was also measured at a reasonable test point to ensure the safety of the designed wireless charging system.

The impact of inductance variation on the power transfer capability was discussed based on an LCL-S compensated IPT system. A frequency modulated MPPT method was proposed to track the maximum power point of the IPT systems by adjusting the operating frequency. The method could track the output power point and improve the output power, which is weakened by the inductance manufacturing tolerances and the coupler misalignment.

The algorithm has been validated and analyzed via simulation in different operating cases. The proposed modulated MPPT method can track the maximum power point by varying the operating frequency of the inverter to improve the output power that is affected by the resonant point drifting. The experimental results of the frequency modulated MPPT method was demonstrated in a low power rating to show the feasibility.

6.2 Future Works

Operate the IPT testbed in different working conditions to validate the power transfer capability and analyze its performance. Add the shielding to the IPT system and evaluate its performance. Measure the EMF in more testing points surrounding the IPT testbed to ensure the emission meet the ICNIRP 2010 standard.

Investigate the optimization method for the IPT system for the railway application to improve its power transfer capability with higher system efficiency and a better misalignment performance.

Continue to analyze the inductor tolerance impact with multiple parameter variations. Add the mission profile of the battery to the system to explore the application of the frequency modulated MPPT method in different load types. Improve the MPPT method in terms of its stability and the transient time. Implement the hardware testing in different working environments to validate the controller performance.

6.3 Publications

My main publications are listed as follows,

1. X. Xu, T. Zhao, S. -E. Chen, N. Braxtan and D. Ward, "A Frequency Modulated Maximum Power Point Tracking Method for Wireless Charging Systems," 2022 IEEE Transportation Electrification Conference & Expo (ITEC), 2022, pp. 285-289.
2. K. Lin, X. Xu, T. Zhao, S. Chen, N. Braxtan, D. Cook, D. Ward, “Optimized Shield Design of an Inductive Power Transfer System for Railway Applications”, 2022 IEEE Transportation Electrification Conference & Expo (ITEC), 2022, pp. 606-610.
3. Best Student Paper Award: X. Xu, L. Wang, K. Lin, T. Zhao, S. Chen, D. Cook, D. Ward, "Design Considerations of An Inductive Power Transfer System for Rail Application," 2021 IEEE Transportation Electrification Conference & Expo (ITEC), 2021, pp. 457-461.
4. Y. Wang, X. Xu and T. Zhao, "An Arcless Step Voltage Regulator based on Paralleled Power Electronics Converter Configuration," 2020 IEEE Applied Power Electronics Conference and Exposition (APEC), 2020, pp. 1006-1011.
5. X. Xu, Y. Wang and T. Zhao, "A Hybrid Switch based Arcless Voltage Regulator," 2018 9th IEEE International Symposium on Power Electronics for Distributed Generation Systems (PEDG), Charlotte, NC, 2018, pp. 1-5.

6. Y. Wang, X. Xu and T. Zhao, "An Arcless Voltage Regulator Based on Hybrid Tap Changing Topology," 2018 9th IEEE International Symposium on Power Electronics for Distributed Generation Systems (PEDG), Charlotte, NC, 2018, pp. 1-4.
7. R. K. Belchandan, X. Xu, E. Shoubaki, M. Manjrekar, T. Zhao, D. Figueroa, R. Kennedy, "Characterization and Performance of 600V 100A Solid-State Circuit Breaker," 2018 9th IEEE International Symposium on Power Electronics for Distributed Generation Systems (PEDG), Charlotte, NC, 2018, pp. 1-4.
8. A. Barthelme, X. Xu and T. Zhao, "A hybrid AC and DC distribution architecture in data centers," 2017 IEEE Energy Conversion Congress and Exposition (ECCE), Cincinnati, OH, 2017, pp. 2017-2022.

REFERENCES

[1] Masson-Delmotte, V. et al, "IPCC Special Report on Global Warming of 1.5 °C", IPCC, 2018. [Online]. Available: https://www.ipcc.ch/sr15/

[2] International Energy Agency (IEA), "The Future of Rail: Opportunities for energy and the environment", in *IEA*, Paris.

[3] Popovich, N.D., Rajagopal, D., Tasar, E. et al., "Economic, environmental and grid-resilience benefits of converting diesel trains to battery-electric." in *Nat Energy 6*, pp: 1017–1025, 2021.

[4] N. Tesla, "Apparatus for transmitting electrical energy.", U.S. Patent *US1119732A*, May 7, 1907. Available: https://patents.google.com/patent/US1119732A/en

[5] F. Lu, H. Zhang, C. Mi, "A Review on the Recent Development of Capacitive Wireless Power Transfer Technology.", in *Energies 2017,* 10, 1752.

[6] M. G. L. Roes, J. L. Duarte, M. A. M. Hendrix and E. A. Lomonova, "Acoustic Energy Transfer: A Review," in *IEEE Trans. Ind. Electron.*, vol. 60, no. 1, pp. 242-248, Jan. 2013.

[7] K. Jin and W. Zhou, "Wireless Laser Power Transmission: A Review of Recent Progress," in *IEEE Trans. Power Electron.*, vol. 34, no. 4, pp. 3842-3859, April 2019.

[8] N. Shinohara, "History and Innovation of Wireless Power Transfer via Microwaves," in *IEEE J. Microw.*, vol. 1, no. 1, pp. 218-228, Jan. 2021.

[9] A. Brecher and D. Arthur, "Review and Evaluation of Wireless Power Transfer (WPT) for Electric Transit Applications," US Dept. of Transp., Washington, DC, USA, FTA Report No. 0060, Aug. 2014.

[10] S. Y. Choi, B. W. Gu, S. Y. Jeong and C. T. Ri m, "Advances in Wireless Power Transfer Systems for Roadway-Powered Electric Vehicles," in *IEEE J. Emerg. Sel. Topics in Power Electron.*, vol. 3, no. 1, pp. 18-36, March 2015.

[11] J. Dai and D. C. Ludois, "A Survey of Wireless Power Transfer and a Critical Comparison of Inductive and Capacitive Coupling for Small Gap Applications," in *IEEE Trans. Power Electron.*, vol. 30, no. 11, pp. 6017-6029, Nov. 2015.

[12] C. C. Mi, G. Buja, S. Y. Choi and C. T. Rim, "Modern Advances in Wireless Power Transfer Systems for Roadway Powered Electric Vehicles," in *IEEE Trans. Ind. Electron.*, vol. 63, no. 10, pp. 6533-6545, Oct. 2016.

[13] A. Ahmad, M. S. Alam and R. Chabaan, "A Comprehensive Review of Wireless Charging Technologies for Electric Vehicles," in *IEEE Trans. Transp. Electrific.*, vol. 4, no. 1, pp. 38-63, March 2018.

[14] D. Patil, M. K. McDonough, J. M. Miller, B. Fahimi and P. T. Balsara, "Wireless Power Transfer for Vehicular Applications: Overview and Challenges," in *IEEE Trans. Transport. Electrific.*, vol. 4, no. 1, pp. 3-37, March 2018.

[15] H. Feng, R. Tavakoli, O. C. Onar and Z. Pantic, "Advances in High-Power Wireless Charging Systems: Overview and Design Considerations," in *IEEE Trans. Transp. Electrific.*, vol. 6, no. 3, pp. 886-919, Sept. 2020.

[16] S. Jayalath and A. Khan, "Design, Challenges, and Trends of Inductive Power Transfer Couplers for Electric Vehicles: A Review," in *IEEE J. Emerg. Sel. Topics in Power Electron.*, vol. 9, no. 5, pp. 6196-6218, Oct. 2021

[17] WiT-3300 FOD System. Accessed: Jan. 1, 2020. [Online]. Available: http://www.terraelectronica.ru/pdf/WITRCITY/WiT-3300DS.pdf

[18] WiTricity Drives EV Interoperability with New 11 kW Wireless Charging System. Accessed: Jun. 28, 2016. [Online]. Available: https://witricity.com/newsroom/press-releases/witricity-drives-ev-interoperability-new-11-kw-wireless-charging-system/

[19] IPT Technology 100kW Charge Bus. [Online]. Available: https://ipt-technology.com/product-ipt-charge-bus-100kw/

[20] J. Tritschler, S. Reichert and B. Goeldi, "A practical investigation of a high power, bidirectional charging system for electric vehicles," in *16th Eur. Conf. Power Electron. Appl.*, pp. 1-7, 2014.

[21] ORNL Demonstrates 120-Kilowatt Wireless Charging for Vehicles. Accessed: Oct. 19, 2018. [Online]. Available: https://www.ornl.gov/news/ornl-demonstrates-120-kilowatt-wireless-charging-vehicles

[22] S. Y. Choi, J. Huh, W. Y. Lee, S. W. Lee, and C.-T. Rim, “New cross-segmented power supply rails for roadway powered electric vehicles,” in *IEEE Trans. Power Electron.*, vol. 28, no. 12, pp. 5832–5841, Dec. 2013

[23] C.-T. Rim, “The development and deployment of on-line electric vehicles (OLEV),” in *Proc. IEEE Energy Convers. Congr. Expo. (ECCE)*, Sep. 2013.

[24] C.-T. Rim, “Trend of roadway powered electric vehicle technology,” in *Mag. Korean Inst. Power Electron.*, vol. 18, no. 4, pp. 45–51, Aug. 2013.

[25] J. Huh, W. Y. Lee, G. H. Cho, B. H. Lee, and C.-T. Rim, “Characterization of novel inductive power transfer systems for on-line electric vehicles,” in *Proc. IEEE Appl. Power Electron. Conf. Expo. (APEC)*, Mar. 2011, pp. 1975–1979.

[26] Bombardier Begins Operation of the First Inductive High Power Charging Station for PRIMOVE Electric Buses. Accessed: Sep. 10, 2013. [Online]. Available: https://bombardier.com/en/media/news/bombardier-begins-operation-first-inductive-high-power-charging-station-primove-electric

[27] WiT-3300 FOD System. Accessed: Nov. 1, 2017. [Online]. Available: http://www.terraelectronica.ru/pdf/WITRCITY/WiT-3300DS.pdf

[28] P. Schumann, T. Diekhans, O. Blum, U. Brenner, and A. Henkel, “Compact 7 kW inductive charging system with circular coil design,” in *Proc. 5th Int. Electr. Drives Prod. Conf. (EDPC)*, Nuremberg, Germany, Sep. 2015, pp. 1–5.

[29] NISSAN Leaf Gen. 2 – for customer, in use since Q4 of 2016. [Online]. Available: http://www.intis.de/wireless-power-transfer.html#projects

[30] R. Bosshard and J. W. Kolar, “Multi-objective optimization of 50 kW/85 kHz IPT system for public transport,” in *IEEE J. Emerg. Sel. Topics Power Electron.*, vol. 4, no. 4, pp. 1370–1382, Dec. 2016.

[31] M. Suzuki et al., “Design method for low radiated emission of 85 kHz band 44 kW rapid charger for electric bus,” in *Proc. IEEE Appl. Power Electron. Conf. Expo. (APEC)*, Mar. 2017, pp. 3695–3701.

[32] J. Pries, V. P. N. Galigekere, O. C. Onar, and G.-J. Su, “A 50-kW three-phase wireless power transfer system using bipolar windings and series resonant networks for rotating magnetic fields,” in *IEEE Trans. Power Electron.*, vol. 35, no. 5, pp. 4500–4517, May 2020.

[33] Wave IPT—Wirelessly Charging Electric Vehicles. [Online]. Available: www.waveipt.com

[34] A. U. Ibrahim, W. Zhong and M. D. Xu, "A 50-kW Three-Channel Wireless Power Transfer System With Low Stray Magnetic Field," in *IEEE Trans. Power Electron.*, vol. 36, no. 9, pp. 9941-9954, Sept. 2021.

[35] Momentum Dynamics. Accessed: Apr. 19, 2018. [Online]. Available: http://www.momentumdynamics.com

[36] L. Xue, V. Galigekere, E. Gurpinar, G. -j. Su and O. Onar, "Modular Design of Receiver Side Power Electronics for 200 kW High Power Dynamic Wireless Charging System," in *2021 IEEE Transp. Electrific. Conf. & Expo (ITEC)*, 2021, pp. 744-748.

[37] J. Huh, S. Lee, C. Park, G. -H. Cho and C. -T. Rim, "High performance inductive power transfer system with narrow rail width for On-Line Electric Vehicles," in *2010 IEEE Energy Conv. Congr. Expo.*, 2010, pp. 647-651

[38] J. Huh, S. W. Lee, W. Y. Lee, G. H. Cho and C. T. Rim, "Narrow-Width Inductive Power Transfer System for Online Electrical Vehicles," in *IEEE Trans. Power Electron.*, vol. 26, no. 12, pp. 3666-3679, Dec. 2011.

[39] Seokhwan Lee et al., "The optimal design of high-powered power supply modules for wireless power transferred train," in *2012 Elect. Syst. Aircr. Railway Ship Propulsion*, 2012, pp. 1-4.

[40] J. Shin, S. Shin, Y. Kim, S. Lee, B. Song and G. Jung, "Optimal current control of a wireless power transfer system for high power efficiency," in *2012 Elect. Syst. Aircr. Railway Ship Propulsion*, 2012, pp. 1-4.

[41] C. H. Lee et al., "Design and introduction of high power transfer system for electrical vehicles," in *2013 IEEE Int. Conf. Intell. Rail Transp. Proc.*, 2013, pp. 280-284.

[42] J. Shin et al., "Design and Implementation of Shaped Magnetic-Resonance-Based Wireless Power Transfer System for Roadway-Powered Moving Electric Vehicles," in *IEEE Trans. Ind. Electron.*, vol. 61, no. 3, pp. 1179-1192, March 2014.

[43] J. H. Kim et al., "Development of 1-MW Inductive Power Transfer System for a High-Speed Train," in *IEEE Trans. Ind. Electron.*, vol. 62, no. 10, pp. 6242-6250, Oct. 2015.

[44] S. Y. Choi, S. Y. Jeong, B. W. Gu, G. C. Lim and C. T. Rim, "Ultraslim S-Type Power Supply Rails for Roadway-Powered Electric Vehicles," in *IEEE Trans. Power Electron.*, vol. 30, no. 11, pp. 6456-6468, Nov. 2015.

[45] Y. Li et al., "Design and implementation of a novel WPT system for railway applications," in *2017 IEEE PELS Workshop Emerg. Technol.: Wireless Power Transfer (WoW),* 2017

[46] L. Wang, T. Zhao, S. -E. Chen and D. Cook, "An Inductive Power Transfer System Design for Rail Applications," in *2018 IEEE Trans. Electrific. Conf. Expo (ITEC)*, 2018, pp. 84-89

[47] C. Anyapo and P. Intani, "Development of Long Rail Dynamic Wireless Power Transfer for High-Speed Train," in *2019 16th Int. Conf. Elect. Eng. /Electron., Comput., Telecommun. Inf. Tech.* (ECTI-CON), 2019, pp. 565-568

[48] C. H. Lee, G. Jung, K. A. Hosani, B. Song, D. -k. Seo and D. Cho, "Wireless Power Transfer System for an Autonomous Electric Vehicle," in *2020 IEEE Wireless Power Transfer Conf. (WPTC)*, 2020, pp. 467-470

[49] B. Song, S. Cui, Y. Li and C. Zhu, "A Narrow-Rail Three-Phase Magnetic Coupler With Uniform Output Power for EV Dynamic Wireless Charging," in *IEEE Trans. Ind. Electron.*, vol. 68, no. 8, pp. 6456-6469, Aug. 2021.

[50] M. Budhia, G. A. Covic, J. T. Boys and C. Huang, "Development and evaluation of single sided flux couplers for contactless electric vehicle charging," in *2011 IEEE Energy Conv. Congr. Expo.*, 2011, pp. 614-621.

[51] G. A. Covic and J. T. Boys, "Modern Trends in Inductive Power Transfer for Transportation Applications," in *IEEE J. Emerg. Sel. Topics Power Electron.*, vol. 1, no. 1, pp. 28-41, March 2013.

[52] J. T. Boys, G. A. J. Elliott and G. A. Covic, "An Appropriate Magnetic Coupling Co-Efficient for the Design and Comparison of ICPT Pickups," in *IEEE Trans. Power Electron.*, vol. 22, no. 1, pp. 333-335, Jan. 2007

[53] Chwei-Sen Wang, O. H. Stielau and G. A. Covic, "Design considerations for a contactless electric vehicle battery charger," in *IEEE Trans.actions Ind. Electron.*, vol. 52, no. 5, pp. 1308-1314, Oct. 2005

[54] Chwei-Sen Wang, G. A. Covic and O. H. Stielau, "Power transfer capability and bifurcation phenomena of loosely coupled inductive power transfer systems," in *IEEE Trans. Ind. Electron.*, vol. 51, no. 1, pp. 148-157, Feb. 2004

[55] Y. Chen, H. Zhang, C. -S. Shin, K. -H. Seo, S. -J. Park and D. -H. Kim, "A Comparative Study of S-S and LCC-S Compensation Topology of Inductive Power Transfer Systems for EV Chargers," in *2019 IEEE 10th Int. Symp. Power Electron. Distrib. Gener. Syst. (PEDG)*, 2019.

[56] Y. Wang, H. Wang, T. Liang, X. Zhang, D. Xu and L. Cai, "Analysis and design of an LCC/S compensated resonant converter for inductively coupled power transfer," in *2017 IEEE Transp. Electrific. Conf. and Expo, Asia-Pacific (ITEC Asia-Pacific)*, 2017.

[57] W. Li, H. Zhao, S. Li, J. Deng, T. Kan and C. C. Mi, "Integrated ${LCC}$ Compensation Topology for Wireless Charger in Electric and Plug-in Electric Vehicles," in *IEEE Trans. Ind. Electron.*, vol. 62, no. 7, pp. 4215-4225, July 2015

[58] Zhou, Wu, Zhang and Dai, "Design and analysis of the LCL resonant convertor in inductive Power Transfer system," in *2014 Int. Power Electron. Appl. Conf. Expo.*, Shanghai, 2014, pp. 1271-1276.

[59] Sweya Sasikumar and K. Deepa, “LCL Topology Based Single Stage Boost Rectifier Topology for Wireless EV”, in *J. Green Eng.*, Vol.8, Issue 4, pp.573 - 596, 2018.

[60] W. Zhang and C. C. Mi, "Compensation Topologies of High-Power Wireless Power Transfer Systems," in *IEEE Trans. Veh. Tech.*, vol. 65, no. 6, pp. 4768-4778, June 2016

[61] R. Tavakoli and Z. Pantic, "Analysis, Design, and Demonstration of a 25-kW Dynamic Wireless Charging System for Roadway Electric Vehicles," in *IEEE J. Emerg. Sel. Topics Power Electron.*, vol. 6, no. 3, pp. 1378-1393, Sept. 2018.

[62] X. Dai, X. Li, Y. Li and A. P. Hu, "Maximum Efficiency Tracking for Wireless Power Transfer Systems With Dynamic Coupling Coefficient Estimation," in *IEEE Trans. Power Electron.*, vol. 33, no. 6, pp. 5005-5015, June 2018.

[63] International Commission on Non-Ionizing Radiation Protection, "Guidelines for limiting exposure to time-varying electric and magnetic fields (1 Hz to 100 kHz)," Health Physics, vol. 99, no. 6, pp. 818–836, Dec. 2010.

[64] IEEE Standard for Safety Levels with Respect to Human Exposure to Radio Frequency Electromagnetic Fields, 3 kHz to 300 GHz, IEEE C95.1-2005. [Online]. Available: https://standards.ieee.org/standard/C95_1-2005.html

[65] Electric vehicle wireless power transfer (WPT) systems, IEC TS 61980. [Online]. Available: https://webstore.iec.ch/searchform&q=IEC%20TS%2061980

[66] Wireless Power Transfer for Light-Duty Plug-in/Electric Vehicles and Alignment Methodology, J2954_202010. [Online]. Available: https://www.sae.org/standards/content/j2954_202010

[67] J. Huh, S. W. Lee, W. Y. Lee, G. H. Cho and C. T. Rim, "Narrow-Width Inductive Power Transfer System for Online Electrical Vehicles," in *IEEE Trans. Power Electron.*, vol. 26, no. 12, pp. 3666-3679, Dec. 2011.

[68] X. Xu et al., "Design Considerations of An Inductive Power Transfer System for Rail Application," *2021 IEEE Transp. Electrific. Conf. Expo (ITEC)*, 2021, pp. 457-461, doi: 10.1109/ITEC51675.2021.9490168.

[69] Magnetic field levels generated by electronic and electrical apparatus in the railway environment with respect to human exposure - Measurement procedures, IEC 62597. [Online]. Available: https://webstore.iec.ch/publication/62750

[70] E. Chaidee, A. Sangswang, S. Naetiladdanon and E. Mujjalinvimut, "Maximum output power tracking for wireless power transfer system using impedance tuning," in *IECON 2017 - 43rd Ann. Conf. IEEE Ind. Electron. Soc.*, pp. 6961-6966, 2017.

[71] Y. Lim, H. Tang, S. Lim and J. Park, "An Adaptive Impedance-Matching Network Based on a Novel Capacitor Matrix for Wireless Power Transfer," in *IEEE Tran. Power Electron.*, vol. 29, no. 8, pp. 4403-4413, Aug. 2014.

[72] M. H. Ameri, A. Yazdian Varjani and M. Mohamadian, "A novel algorithm for tracking maximum inductive transferred power point," in *4th Annu. Int. Power Electron., Drive Syst. Technol. Conf.*, pp. 372-377, 2013.

[73] Y. Wang, A. a. Mostafa, H. Zhang, Y. Mei, C. Zhu and F. Lu, "Sensitivity Investigation and Mitigation on Power and Efficiency to Resonant Parameters in an LCC Network for Inductive Power Transfer," in *IEEE J. Emerg. Sel. Topics Power Electron.*, doi: 10.1109/JESTIE.2021.3118274.

[74] X. Xu, T. Zhao, S. -E. Chen, N. Braxtan and D. Ward, "A Frequency Modulated Maximum Power Point Tracking Method for Wireless Charging Systems," in *2022 IEEE Transp. Electrific. Conf. Expo (ITEC)*, 2022, pp. 285-289

[75] K. Lin, X. Xu, T. Zhao, S. Chen, N. Braxtan, D. Cook and D. Ward, "Passive Shielding Design of an Inductive Power Transfer System for Railway Applications," in *2022 IEEE Transp. Electrific. Conf. Expo (ITEC)*2022, pp. 606-610